Article:
Ramirez, JA, Peleg, N, Baird, AJ orcid.org/0000-0001-8198-3229 et al. (4 more authors) (2023) Modelling peatland development in high-boreal Quebec, Canada, with DigiBog_Boreal. Ecological Modelling, 478. 110298. ISSN 0304-3800

https://doi.org/10.1016/j.ecolmodel.2023.110298

Modelling peatland development in high-boreal Quebec, Canada, with DigiBog_Boreal

Jorge A. Ramirez[a,b*], Nadav Peleg[c], Andy J. Baird[d], Dylan M. Young[d], Paul J. Morris[d], Marie Larocque[e], Michelle Garneau[a]

[a]GEOTOP and GRIL research centers; Department of Geography, Université du Québec à Montréal, Montréal, Canada
[b]Department of Geography, University of Exeter, Exeter, UK
[c]Institute of Earth Surface Dynamics, University of Lausanne, Lausanne, Switzerland
[d]School of Geography, University of Leeds, Leeds, UK
[e]GEOTOP and GRIL research centers; Département des Sciences de la Terre et de l'Atmosphère, Université du Québec à Montréal, Montréal, Canada

*corresponding author (j.a.ramirez@exeter.ac.uk)

Abstract

DigiBog is a numerical model that simulates peat accumulation in temperate peatlands. Here, we modify DigiBog for boreal peatlands (DigiBog_Boreal) by accounting for snow cover, short growing seasons and groundwater exchanges between the peat and the aquifer. DigiBog_Boreal is then used to replicate ~6500 years of peat accumulation at two high boreal latitude peatlands in Quebec, Canada. DigiBog_Boreal was driven with a weather generator and climate models, while peat cores from the sites were used to develop initial conditions and calibrate DigiBog_Boreal. Our results demonstrate that DigiBog_Boreal can replicate well peat thickness and age-depth profiles but cannot produce long-term fluctuations in water-table depths. Here, a possible explanation for DigiBog_Boreal's underperformance is the stability in the climatic drivers and less likely the new model developments. The results also indicate that peat decomposition and accumulation in DigiBog_Boreal are sensitive to water stored on the peat surface.

Keywords

peatland, DigiBog model, high boreal latitudes, ecohydrology, Holocene, carbon dynamics

1. Introduction

Peatlands form where net primary production exceeds organic matter decomposition, resulting in the accumulation of peat and carbon (C) (Wieder and Vitt, 2006). Northern peatlands in temperate, boreal, and Arctic regions cover 3.7 ± 0.5 million km^2, and store 415 ± 150 Pg of C (Hugelius et al., 2020). Globally, the majority of peatlands are

found in the boreal biome (Joosten and Clarke, 2002), where 15% of the land cover is peatland (Xu et al., 2018).

Numerical models are useful in helping to identify the processes and conditions that underpin peatland development. Regional- to global -scale models (Chaudhary et al., 2017; Müller and Joos, 2020) have been applied to boreal peatlands and provide a mesoscale (100s km) view of carbon stock changes, but they lack the fine spatial resolution (tens of m) needed to represent variations in peat properties and landscape setting, both of which can strongly influence peatland hydrological processes and peatland development (e.g., Qiu et al., 2019). Models that can be applied at the finer scale of individual peatlands include DigiBog, Holocene Peat Model (HPM), and MPeat (Baird et al., 2012; Frolking et al., 2010; Mahdiyasa et al., 2021; Morris et al., 2012). With the exception of DigiBog, these models reduce an entire peatland into a single column of peat (i.e., they are one-dimensional). However, although DigiBog can simulate peatlands in two and three dimensions, it was built for temperate climates and cannot account for snow cover and the short growing seasons found in boreal regions, unlike HPM (Treat et al., 2021). Therefore, we updated DigiBog to create a new version of the model – DigiBog_Boreal – which we describe here. We also report on the application of the two-dimensional version of DigiBog_Boreal to two high boreal peatlands in northeastern Canada. Finally, we comment on the difficulties of reconstructing past boundary conditions required to drive the model, and the effect of boundary condition uncertainty on model accuracy.

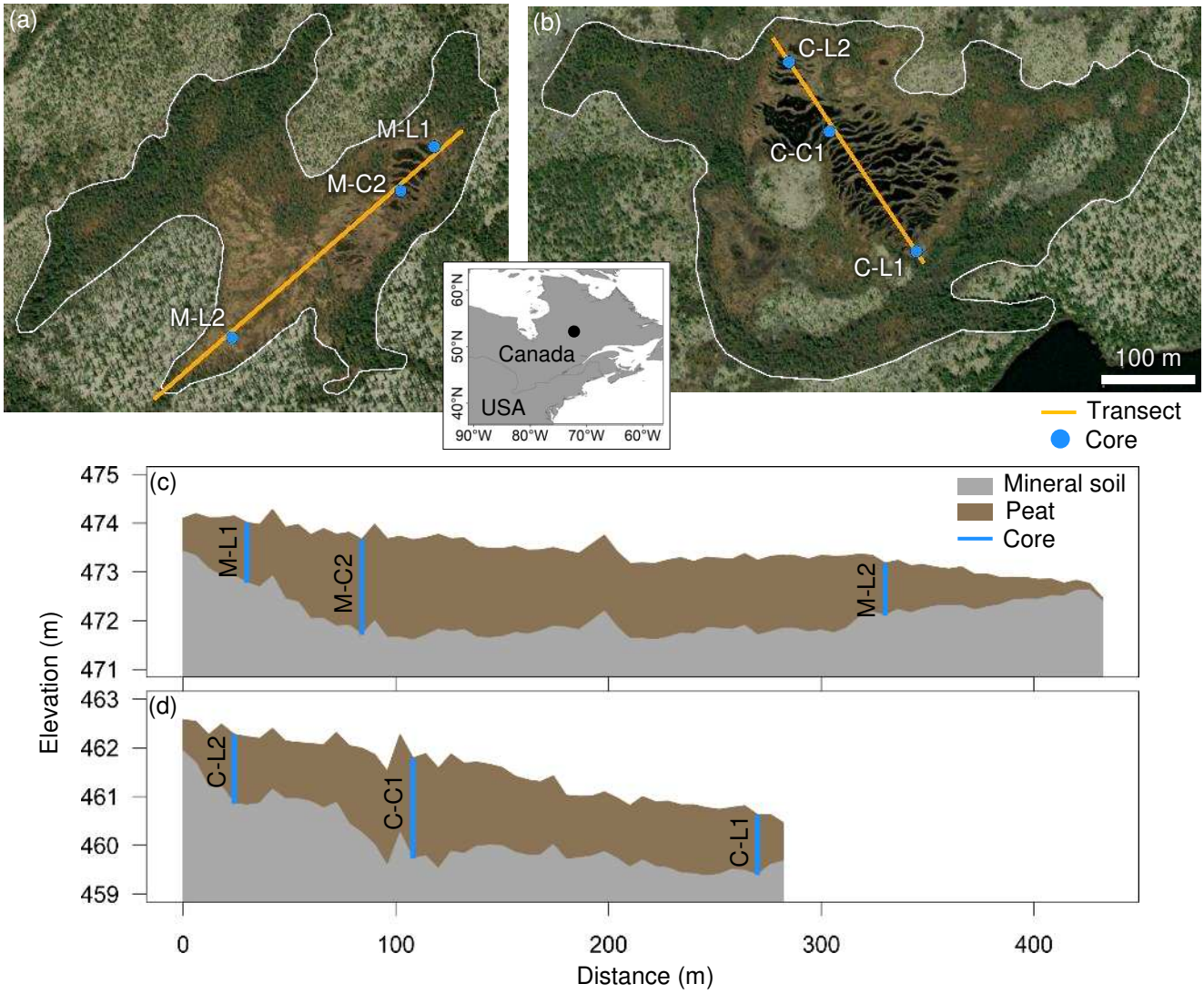

Figure 1. Location and profile view of modelled transects and observed core locations at Misask (a, c) and Cheinu (b, d). White line is the peatland boundary.

2. Study Area

The two peatlands used to test DigiBog_Boreal are located in separate watersheds north of the Otish Mountains in north-central Quebec. They were originally selected to document their current hydrological dynamics (Lambert et al., 2022) and Holocene ecohydrological trajectories in response to climate variations (Robitaille et al., 2021). These peatlands are called Misask (52°43′27″N, 72°12′50″W) and Cheinu (52°38′48″N, 72°11′31″W) and have areas of 0.102 and 0.148 km^2, respectively (Fig. 1 a, b). Both sites are in the Dfc (cold, no dry season, cold summer) class of the Köppen-Geiger climate map produced by Beck et al. (2018). Misask is partially patterned with a microtopography of alternating low hummocks, lawns, wet hollows and pools covering approximately 10% of its total area (Robitaille et al., 2021). Cheinu is characterized by a patterned surface with elongated and parallel pools covering up to 60% of the total

area. Both peatlands have developed in local depressions within the post-glacial landscape and are underlain by boulders and sand-filled interstices inherited from till leaching (Fig. 1 c, d). Both sites are dominated by *Sphagnum* spp. and show evidence of recent lateral peatland expansion (Robitaille et al., 2021). *Carex spp.* and *Trichophorum cespitosum* are the herbaceous species mostly found in depressions while ericaceous taxa like *Chamaedaphne calyculata* and *Kalmia angustifolia* are located on strings (Robitaille et al., 2021). Along the edges of the sites there are black spruce (*Picea mariana*) and larch (*Larix laricina*) trees.

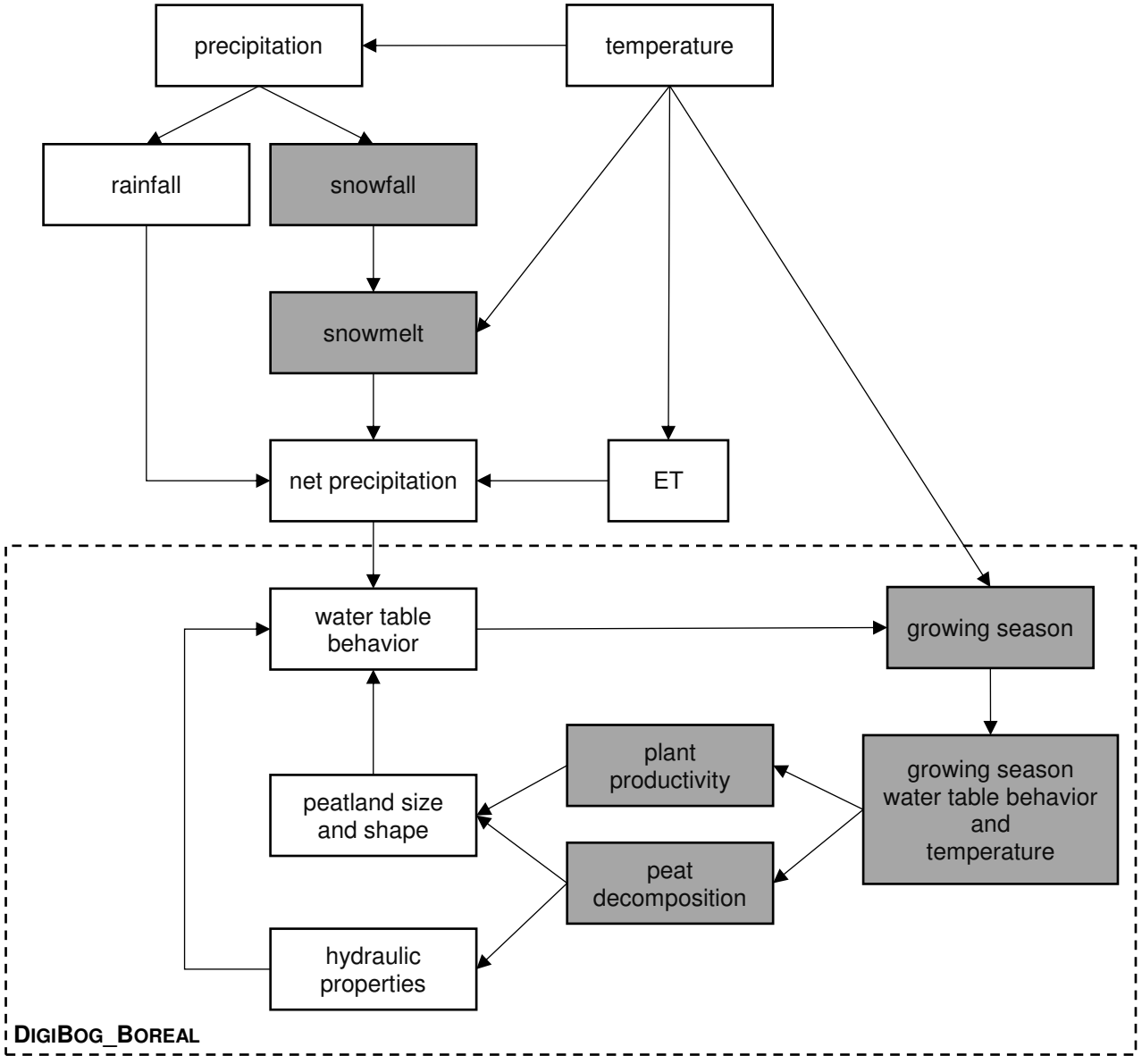

Figure 2. A schematic of DigiBog_Boreal (adapted from Morris et al., 2015) where boxes shaded in grey are new inputs and adapted processes in DigiBog.

3. Methods and Data

3.1 Developing DigiBog_Boreal

DigiBog is a process-based model of peatland development (Baird et al., 2012; Morris et al., 2012) and has been applied to northern temperate peatlands (Young et al., 2017). DigiBog has submodels that simulate plant litter production, peat decomposition, peat hydraulic properties, and water-table behavior (Fig. 2). The new version – DigiBog_Boreal – considers the effects of a boreal climate on peatland development by: 1) limiting plant production, and so the formation of new litter, to the growing season, based on growing season temperatures and water-table behavior; 2) limiting peat decomposition to the growing season in a similar manner; and 3) including a representation of snow accumulation and melt, which are important parts of the hydrological cycle in the boreal biome (Fig. 2).

In common with the earlier versions of DigiBog described by Baird et al. (2012), Morris et al. (2012) and Young et al. (2017), DigiBog_Boreal represents a peatland as multiple adjacent columns of peat, between which water can flow in response to local water-table gradients. Peat properties can vary vertically within individual columns – each column has layers – or horizontally between them. The initial condition of the model is a mineral soil topography upon which peat subsequently accumulates if conditions allow. Litter production depends on air temperature and water-table depth below the surface, with cohorts of new litter being added annually to the top of each column (the peat surface) at the rate p (kg m^{-2} yr^{-1}) (Morris et al., 2015). Annual average air temperatures for boreal peatlands are usually less than 0 °C (Garneau et al., 2014; Moore, 1989), and would result in no litter production if DigiBog's existing plant productivity function was used; this is because the function is based on data from a peatland in an oceanic temperate climate with long growing seasons. Therefore, DigiBog's annual litter production equation (Morris et al., 2015) was modified to reflect the temperature of the growing season under boreal conditions and the proportion of the year occupied by the growing season. The modified litter production equation thus becomes:

$$p = \left(0.001\left(9.3 + 133Z_{gs} - 0.022\left(100Z_{gs}\right)^2\right)^2\left(0.1575T_{AVEgs} + 0.0091\right)\right)t_{gs} \quad (1)$$

for $0\ \text{m} \leq Z_{gs} \leq 0.668\ \text{m}$, and $p = 0$ where $Z_{gs} > 0.668\ \text{m}$

where the average growing season temperature (T_{AVEgs}, °C) replaces average annual air temperature, average growing season oxic zone thickness (given by water-table depth) (Z_{gs}, m) replaces average annual oxic zone thickness, and litter production is reduced by the proportion of the year occupied by the growing season (t_{gs}). Constants in the litter production equation presented in Morris et al. (2015) remain unchanged, and were derived from empirical data sets (Belyea and Clymo, 2001; Breeuwer et al., 2008).

Peat decomposition in DigiBog_Boreal is also dependent on air temperature, water-table depth and the recalcitrance of peat. The latter, increases as peat becomes more decomposed (Young et al., 2017). Decomposition is calculated on a weekly time scale as a change in each peat layer's mass (M_t, kg m^{-2}). As opposed to year-round decomposition in DigiBog, DigiBog_Boreal assumes that decomposition only occurs during the growing season, calculated on a weekly basis. Hence, DigiBog's peat decomposition equation was modified to the following:

$$M_t = M_{t-1}\left[\left(ox \cdot e^{-\Delta t m_{ox}\alpha_{ox,T_{BC}}\,Q_{10}^{(T_{AVEgs}-T_{BC})/10}}\right) + \left(an \cdot e^{-\Delta t m_{an}\alpha_{an,T_{BC}}\,Q_{10}^{(T_{AVEgs}-T_{BC})/10}}\right)\right] \quad (2)$$

where the average growing season temperature (T_{AVEgs}, °C), replaces average annual air temperature. The remaining parameters are unchanged and include *ox* and *an* as the proportions of the layer occurring above and below the water table respectively. α_{ox} and α_{an} are user-set decay parameters for oxic and anoxic conditions, Q_{10} is a temperature sensitivity parameter, T_{BC} = 6.29 °C is a baseline temperature, and m_{ox} and m_{an} are user-set degrees of recalcitrance for peat under oxic and anoxic conditions (Morris et al., 2015).

Water movement in DigiBog_Boreal occurs between peat columns at sub-hourly time steps to maintain numerical stability. Water movement is affected by changes in peat saturated hydraulic conductivity which changes according to the degree of peat decomposition (Young et al., 2017). Water is also allowed to pond on the surface of a modelled peatland to a depth defined by the user (see Baird et al. 2012) and once the stored water exceeds the threshold depth, it is lost from the model domain (which is akin to rapid overland flow to the peatland margin). Groundwater recharge is based on net precipitation, which is rainfall + snowmelt – evapotranspiration. In high-latitude

boreal peatlands in northern Quebec, surficial peat seasonally freezes (Kingsbury and Moore, 1987) and large amounts of snowmelt occur at the onset of the growing season (Quinton and Roulet, 1998). Our modelled peatland subsurface received no precipitation during the winter because the surface of the peatland was assumed frozen. Snowfall simply accumulates during the period where temperatures are < 0°C and snowmelt is added to precipitation in the spring when temperatures rise above freezing. DigiBog_Boreal does not explicitly model snow processes and a separate snowmelt model is used, as explained in section 3.2.2.

3.2 DigiBog_Boreal setup for the study sites

For this study, DigiBog_Boreal was driven with modelled climate data. We used field observations to establish initial conditions and to calibrate the model (Fig. S1).

3.2.1 Atmospheric boundary conditions

In 2016, three peat cores were obtained at each site (Fig. 1 a-d) for paleoenvironmental reconstructions (see Robitaille et al. (2021) for more details). Radiocarbon dates from the base of these cores indicate that the Misask and Cheinu peatlands initiated at least 6500 calibrated years before present (cal. yr BP). Therefore, time series inputs for DigiBog_Boreal ran from 6500 cal. yr BP to 2016 Common Era (CE). Climate inputs to DigiBog_Boreal are time series of net precipitation at a weekly resolution and average growing season temperature per annum. Actual evapotranspiration (AET) was not used in the net precipitation calculation, but potential evapotranspiration (PET) was used instead. At our sites the difference between PET and AET should be minimal because observed water-table depths are shallow (< 7 cm) and at these depths PET is approximately the same as AET (e.g. Kim and Verma, 1996; Wu et al., 2010).

To obtain climate inputs for DigiBog_Boreal, we used the AWE-GEN weather generator model (Fatichi et al., 2013, 2011) that enables the simulation of precipitation, temperature and potential evapotranspiration while preserving the cross-correlations between the simulated variables. The model was first calibrated for the present period, and then its parameters were modified using information from climate models with the "factors of change" (FC) approach (e.g. Moraga et al., 2021) to simulate the climate conditions of the past (Fatichi et al., 2021). The model was calibrated with ERA5 climate re-analysis data (Hersbach et al., 2020) for the period 1981 to 2019 CE and

validated with adjusted daily precipitation and temperature from 1943 to 1983 CE (Wang et al., 2017) acquired from the nearest weather station, Nitchequon, which lies 100 km northeast from Misask and Cheinu (Fig. S2 a-b). The use of different data for calibration and validation ensures the independence of the validation procedure. Modelled monthly PET was calibrated with PET derived from daily ANUSPLIN temperature (1950-2017 CE) (McKenney et al., 2011) using the Hamon method (Hamon, 1961) as proposed by Oudin et al. (2005) (Fig. S2 c).

The general circulation model HadCM3 (Gordon et al., 2000; Valdes et al., 2017) provided the underlying climate from 6500 cal. yr BP to 1950 CE for the AWE-GEN paleoclimate reconstruction. Two FC were used, a difference in air temperature between the reference period (1950 CE ±15 yr) and the simulated period and the ratio of average precipitation intensity between the two periods (for further discussion on the FC method see Peleg et al. (2019) and Moraga et al. (2021)). Seasonal FC were computed at intervals of 500 years and applied on 50-year intervals using linear interpolation between each of the 500-year points (Fig. S2 d-e). No FC for PET were computed because the AWE-GEN modeled paleoclimate PET is directly conditioned on temperature. The final output from our method was 6566 years of daily average temperature, precipitation, and evapotranspiration, where 6500 cal. yr BP to 1950 CE simulates the past climate and the calibrated period of 1950 to 2016 CE represents the present climate.

Temperature thresholds were used to define the growing season at the sites. As proposed by Christidis et al. (2007), thresholds for spring (T_S) and autumn (T_A) were applied to smoothed daily average temperatures, determined with a low pass filter (itsmr package version 1.9 in R version 3.6.1), to define the growing season while unsmoothed daily average temperatures were used to calculate the average growing season temperature (Fig. S3 a). The growing season begins on the first day when the smoothed daily average temperature is greater than T_S and ends on the first day the smoothed daily average temperature is less than T_A. For our sites, the onset of spring and the end of autumn used temperature thresholds of T_S = 10 °C (Lottes and Ziegler, 1994) and T_A = 6 °C (Fig. S3 a). The capacity of these thresholds to determine the growing season was tested using 7000 years of AWE-GEN present-day climate (1981-2019 CE) smoothed with a low pass filter. The resulting growing seasons: 1) mostly

start in early June and end in late September, 2) have lengths between 95 and 123 days, and 3) average temperatures near 12 °C (Fig. S3 b-d). For our sites, the temperature threshold method employed produced present-day growing season lengths that are comparable to those derived using machine learning methods (81-100 days) (Pedlar et al., 2015). These thresholds were applied to the 6566 years of daily average temperatures to determine the average growing season temperature and the weeks of the year for growing season commencement and conclusion.

3.2.2 Hydrological boundary conditions

Snowmelt contributes to the growing season hydrology of Misask and Cheinu, and was modelled using a degree-day method (DDM) developed in the MAC-HBV hydrological model (Samuel et al., 2011). A DDM was chosen because it has low data requirements, and parameter values for the LaGrande River catchment, located 50 km north of our study site, were available as a starting point for model calibration (Agnihotri and Coulibaly, 2020) (Table S1). The DDM requires average daily precipitation and temperature observations as input and produces modelled rainfall, snowfall, and snowmelt as output. For model calibration (Table S1), the DDM was driven with 7000 years of AWE-GEN present-day climate (1981-2019 CE). The DDM-modelled rainfall and snow water equivalent (SWE) were compared to weather observations measured at the Nitchequon weather station from 1943 to 1983 CE (Wang et al., 2017). The calibrated DDM adequately replicated the weekly (Fig. S4 a, b) and annual (Fig. S4 d, e) rainfall and SWE. Moreover, the modelled snowmelt began in April, peaked in May and concluded in June (Fig. S4 c) and this timing was mirrored in hydrographs obtained from a gauging station 200 km downstream from the study site (Fig. S4 c). To determine past and present-day daily rainfall and snowmelt, the calibrated DDM model was driven with the 6566 years of simulated daily average temperature and precipitation. Modelled snowmelt and rainfall were combined with evapotranspiration to produce net precipitation and resampled to a weekly resolution for input into DigiBog_Boreal (Fig. S1).

For the Misask and Cheinu peatlands, exchanges of water between the peat and the underlying aquifer were included because Lambert et al. (2022) showed that both sites are flow-through peatlands receiving groundwater at their upstream portions and discharging water to the aquifer at their downstream limit. Groundwater fluxes in

DigiBog_Boreal were replicated by removing or adding a constant rate of water flow from each column of peat throughout the simulation. Groundwater fluxes along the transect were determined by linearly interpolating values between the endpoints with minimum and maximum amounts of groundwater flux (Fig. S5 a, b). For example, a simulation with ± 100 mm yr^{-1} groundwater flux would gain 100 mm yr^{-1} of groundwater at the most upslope location on the transect and lose 100 mm yr^{-1} of groundwater at the most downslope location. In total, five scenarios were tested for each site (Fig. S5 a, b), with 0, ± 25, ± 50, ± 75, and ± 100 mm yr^{-1} of groundwater flux. These values are based on field measurements and simulated fluxes estimated by Lambert et al. (2022). For all simulations, and at both sites, the DigiBog_Boreal calibration (section 3.2.4) used the ± 100 mm yr^{-1} groundwater flux. The remaining scenarios were applied to the calibrated model to determine the sensitivity of DigiBog_Boreal to groundwater fluxes.

3.2.3 Initial conditions

In 2016 CE, peat thicknesses were surveyed at Misask (n = 116 locations) and Cheinu (n = 167) via manual probing (Robitaille et al, 2021). Additionally, a 1 m spatial resolution digital elevation model (DEM) was produced for each site by applying photogrammetric methods to approximately 2500 overlapping images acquired from a drone (Lambert et al., 2022). Peat thickness data were spatially interpolated using the Topo to Raster function in ArcGIS 10.5 to produce peat depth maps, and the top of the mineral soil at each site was inferred by subtracting peat depths from the DEM (Lambert et al., 2022). Downward sloping transects that nearly intersect each core and terminated near the peatland boundary were digitized for each site (Fig. 1 a, b). Transects were also chosen such that lateral flows perpendicular to them were minimal; this reduces the possibility that transects are accumulating or shedding flow. The transect length for Misask was 432 m and 282 m for Cheinu. Along these transects mineral surface elevation was extracted with a horizontal resolution of 6 m and resulted in 75 and 50 interacting peat columns for Misask and Cheinu respectively (Fig. 1 c, d). These mineral surfaces were representative of the landscape at 6500 cal. yr BP and were the initial conditions for the DigiBog_Boreal simulations. The upslope end of each transect was set to have no-flow (Neumann condition) and the downslope end a constant water level with respect to the peat surface (a Dirichlet condition).

3.2.4 Calibration

For both sites, measurements obtained from the 2016 CE field campaign and follow-up laboratory work were used to calibrate DigiBog_Boreal. The data that were used were: 1) present-day (2016 CE) peat heights across the transect extracted from the DEM (Fig. 1 c, d), 2) peat chronologies (age-depth curves), 3) reconstructed water-table depths (WTD), and 4) a measure of peat mass remaining. In the model, the degree to which peat has decayed or decomposed is given for each layer as the current mass of the layer divided by its original mass; this is what we term as peat mass remaining. Items 2, and 3 (above) were obtained for three cores per site and item 4 from cores M-C2 and C-C1 (Fig. 1 a, b). The cores were 114-199 cm long and spanned the period from 6476 cal. yr BP to 2016 CE. Radiocarbon dating was performed on 43 peat samples from the cores to develop peat age-depth models and analyzed at 4 cm intervals to reconstruct WTD. Carbon to nitrogen ratios (C:N), a proxy for peat mass remaining, was measured for cores M-C2 and C-C1 (see Robitaille et al. (2021) for methods). The parameters that were calibrated in DigiBog_Boreal were: 1) rate of oxic (α_{ox}) and anoxic (α_{an}) peat decomposition, 2) degree of peat recalcitrance under oxic (m_{ox}) and anoxic (m_{an}) conditions, and 3) ponding thickness (see section 3.1). Table S2 contains the parameters that were not calibrated. For both sites, trial and error calibration was performed across the period 6500 cal. yr BP to 2016 CE and was guided by reducing the weighted mean normalized root mean squared error (*wmNRMSE*) between observed and modelled values using the following equation:

$$wmNRMSE = 0.5 \times NRMSE_{PH} + 0.056 \times NRMSE_{PA1} + 0.056 \times NRMSE_{PA2} + 0.056 \times NRMSE_{PA3} + 0.056 \times NRMSE_{WTD1} + 0.056 \times NRMSE_{WTD2} + 0.056 \times NRMSE_{WTD3} + 0.167 \times NRMSE_{MR} \quad (3)$$

where the normalized root mean squared error (*NRMSE*) is expressed as a percentage, with a value of zero being optimal, and is calculated using the present-day peat heights across the transect ($NRMSE_{PH}$), peat age-depth profiles ($NRMSE_{PA}$), WTD ($NRMSE_{WTD}$), and peat mass remaining ($NRMSE_{MR}$). Weights for the *wmNRMSE* were 0.5 for peat heights, which places greater importance on matching the present-day peat surface, and the remaining weights were evenly distributed across the remaining variables.

4. Results

4.1 Climate, weather, and snowmelt model

Table 1 provides summary statistics for the hydrological and meteorological variables (aggregated to an annual resolution) from the data that drove all DigiBog_Boreal simulations at both sites (Fig. 3 a-g). Overall, across the entire period, the simulated climate becomes noticeably wetter and warmer, with minimal changes in snowmelt, evapotranspiration, average growing season temperature, and growing season length (Table 1). From 6500 cal. yr BP to 1850 CE the climate is cooler than present, with shorter growing seasons (Table 1). Recent changes from 1850 CE to 2016 CE include a noticeable increase in average annual temperature, average growing season temperature, and growing season length (Table 1). Throughout this recent period, changes in net precipitation are negligible because increases in rainfall are largely offset by increases in evapotranspiration and decreases in snowmelt (Table 1).

Table 1. Summary statistics of past and present annual hydrometeorological variables presented in Figure 3. Q_1 and Q_3 are the lower and upper quartiles of the data. All (6500 cal. yr BP to 2016 CE), past (6500 cal. yr BP to 1850 CE), and recent (1850 CE to 2016 CE) absolute changes in hydrometeorological variables were derived from the smoothed annual values produced with a locally-weighted polynomial regression. Changes reported in units of variable. GS is growing season.

	min	Q_1	median	Q_3	max	absolute change		
						all	past	recent
rainfall (mm yr^{-1})	307	506	551	599	792	159	103	55
snowmelt (mm yr^{-1})	419	313	356	402	609	4	22	-18
evapotranspiration (mm yr^{-1})	344	381	390	398	439	9	-18	27
net precipitation (mm)	187	454	519	588	910	150	131	19
average annual temperature (^{0}C)	-5.1	-2.7	-2.1	-1.5	1.0	1.0	0.1	0.9
average GS temperature (^{0}C)	10.6	12.3	12.7	13.1	15.0	0.2	-1.2	1.3
growing season length (days)	93	111	113	116	127	5	-5	10

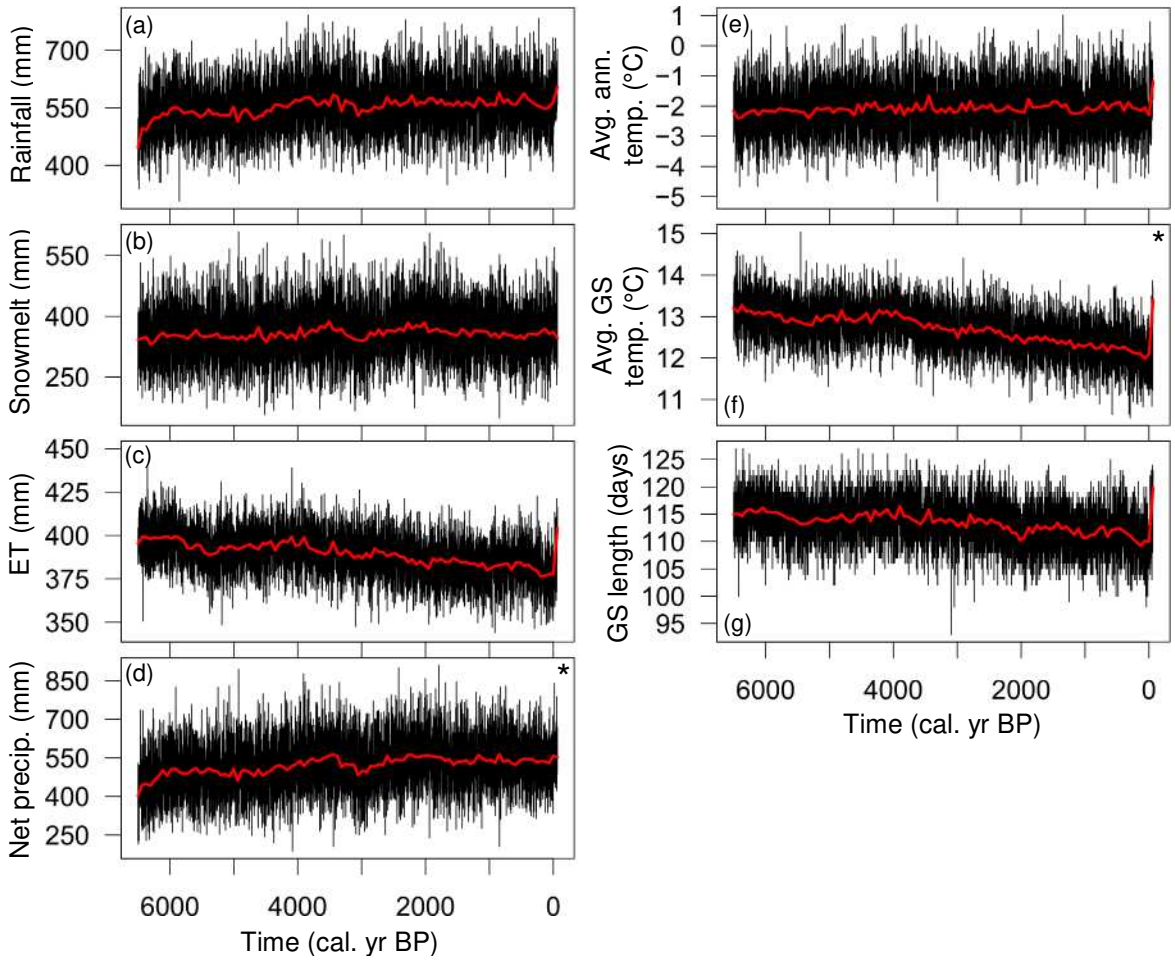

Figure 3. Annual hydrological (a-d) and meteorological (e-g) related variables derived from the daily-resolution AWE-GEN output. Plots denoted with an asterisk are DigiBog_Boreal inputs. ET is evapotranspiration, ann is annual and GS is Growing Season. Red lines are smoothed values produced with a locally-weighted polynomial regression.

4.2 DigiBog_Boreal

4.2.1 Calibration

Table 2 summarizes the optimal model parameterizations and corresponding model error at both sites for simulations with small (run 1) and large (run 2) ponding thicknesses. Overall, the Cheinu simulations were marginally better than the Misask simulations and the run-1 parameterisations performed better than the run 2s (Table 2). For both sites and all runs, peat heights and peat ages were better replicated than WTD and peat mass remaining (Table 2). At Misask, for both run 1 and 2, midslope peat heights were adequately replicated, while upslope peat heights were slightly underestimated and downslope peat heights were substantially overestimated (Fig. 4 a, c, Table 3). Overall, DigiBog_Boreal does quite well for peat height replication at

Cheinu. Peat heights for both runs at Cheinu, were replicated well in the upslope and midslope, with a slight overestimation in the downslope (Fig. 5 a, c, Table 3).

Table 2. Optimal parameterization for DigiBog_Boreal and resulting error between simulated and observed peatland properties at both sites. NRMSE is Normalized Root Mean Square Error, wNRMSE is weighted Normalized Root Mean Square Error, obs is observation, PH is peat height, PA is peat ages, WTD is water table depth and PMR is peat mass remaining.

run	pond thickness (cm)	decay rate parameter (yr^{-1})		degree of peat recalcitrance		obs type	NRMSE (%)				wNRMSE (%)
		anoxic	oxic	anoxic	oxic		PH	PA	WTD	PMR	
Misask 1	0.25	0.0002	0.0425	0.05	0.05	transect	16	—	—	—	20
						M-L1	—	36	31	—	
						M-C2	—	8	25	26	
						M-L2	—	8	31	—	
Misask 2	20	0.0004	0.0425	0.05	0.05	transect	20	—	—	—	27
						M-L1	—	66	30	—	
						M-C2	—	7	38	39	
						M-L2	—	13	38	—	
Cheinu 1	0.25	0.00015	0.0425	0.05	0.05	transect	10	—	—	—	18
						C-L1	—	7	30	—	
						C-C1	—	18	29	25	
						C-L2	—	35	37	—	
Cheinu 2	20	0.00015	0.0425	0.05	0.05	transect	12	—	—	—	20
						C-L1	—	5	26	—	
						C-C1	—	24	37	28	
						C-L2	—	56	29	—	

Table 3. Error in simulated peat heights and summary statistics for simulated peat mass remaining and simulated growing season water-table depths. Values provided for the entire profile and locations on the profile are demarcated in Figure 4 and 5.

run	position	peat mass remaining (%)		average growing season water-table depth (cm)		peat height RMSE (cm)
		avg.	stdev.	avg.	stdev.	
Misask 1	profile	30	19	4	5	36
	upslope	18	19	8	4	14
	midslope	35	17	3	4	25
	downslope	20	19	8	5	57
Misask 2	profile	53	26	-3	8	41
	upslope	28	23	5	7	21
	midslope	60	23	-7	6	27
	downslope	43	23	1	6	68
Cheinu 1	profile	25	17	6	5	26
	upslope	18	17	7	5	20
	midslope	31	16	4	5	19
	downslope	23	16	6	5	34
Cheinu 2	profile	35	20	0	8	29
	upslope	24	22	5	7	13
	midslope	40	17	-2	7	20
	downslope	37	20	-2	9	42

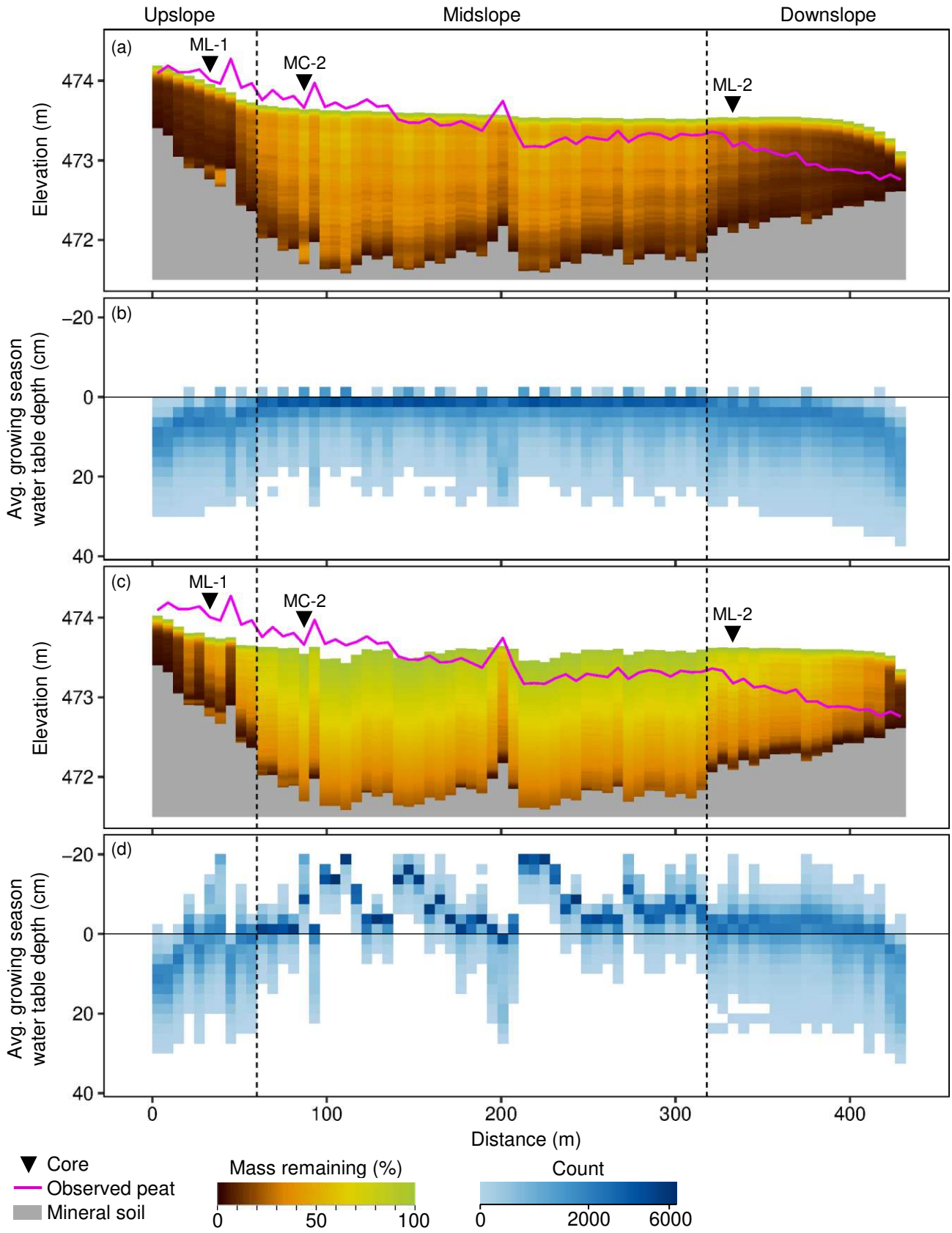

Figure 4. Profile view of present-day simulated peat elevations, simulated peat mass remaining, and observed peat elevations for Misask run 1 (a) and 2 (c). Gradient plots depict the simulated average growing season water-table depths (n = 6566) for each modelled column of peat for Misask run 1 (b) and 2 (d).

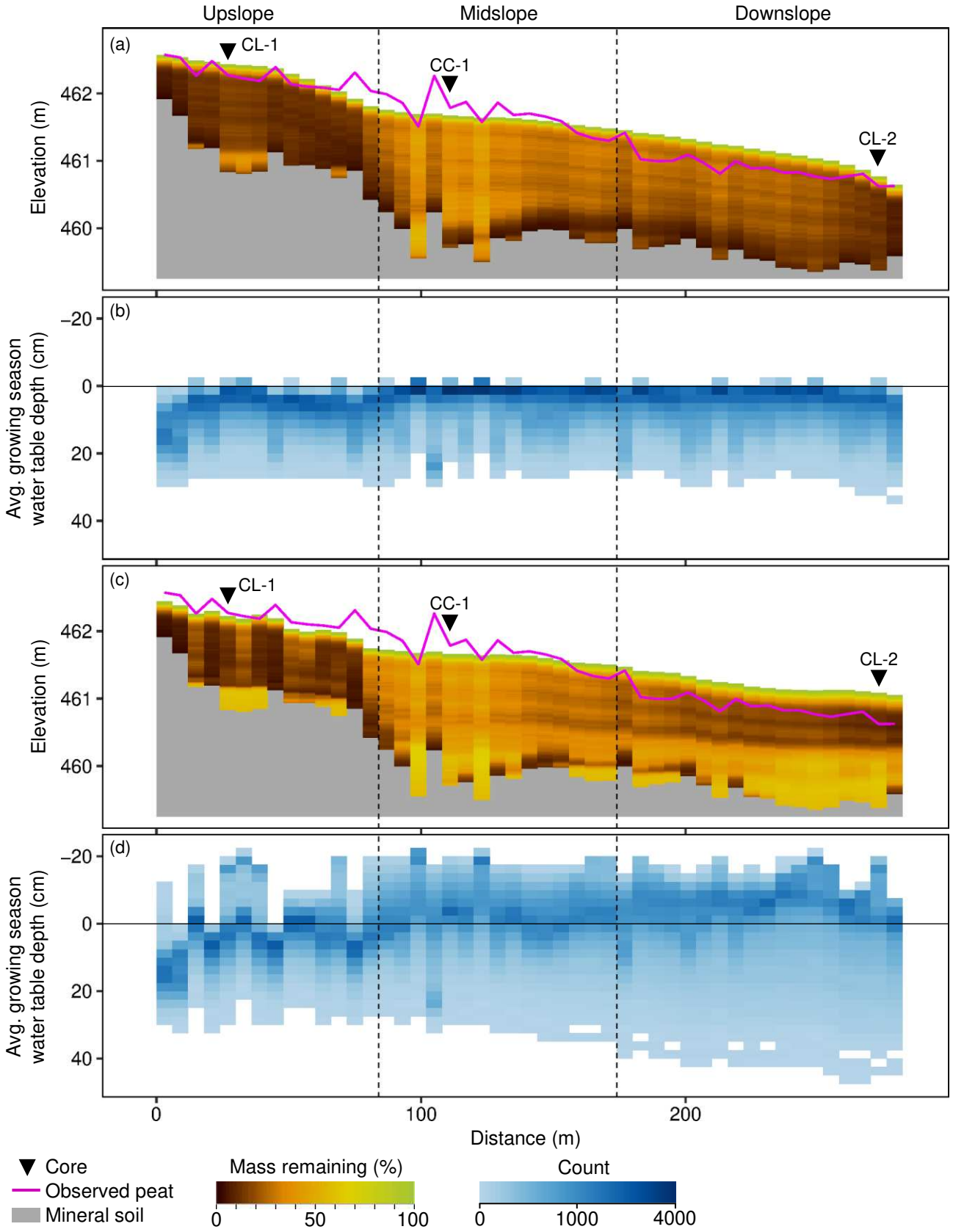

Figure 5. Profile view of present-day simulated peat elevations, simulated peat mass remaining and observed peat elevations for Cheinu run 1 (a) and 2 (c). Gradient plots depict the simulated average growing season water-table depths (n = 6566) for each modelled column of peat for Cheinu run 1 (b) and 2 (d).

Peat age-depth values from simulated profiles at Misask (Fig. 6) contained curvature, while simulated profiles from Cheinu were mostly linear in shape (Fig. 7). At both sites, the run-1 parameterisations were, on average, somewhat better at replicating observed peat age-depth profiles than run 2s (Table 2). DigiBog_Boreal reproduced well peat age-depth profiles for Misask's midslope core MC-2 and lateral core ML-2 (Fig. 6), and Cheinu's downslope core CL-1 (Fig. 7). At all core locations the simulated WTDs were mostly within one standard deviation of the observed mean WTDs, but major changes in observed WTDs were not captured by DigiBog_Boreal (Fig. 6, 6). Misask run 1 and 2, and Cheinu run 1 produced WTDs that largely remained stable. In contrast, the lateral cores (CL-1 and CL-2) from Cheinu run 2 had WTDs that started above the peat surface and then deepened, while WTDs at the central core were above the peat surface and stable (Fig. 7). At Misask 1, below 120 cm the simulated peat decomposition was overestimated (RMSE = 22 percentage points (pp)), while decomposition in shallower layers was underestimated (RMSE = 25 pp) (Fig. 6). Misask run 2 did not replicate observed peat decomposition well (RMSE = 36 pp) (Fig. 6). Cheinu runs 1 and 2 mirrored observed patterns of peat decomposition, but moderately underestimated decomposition (run 1 RMSE = 15 pp, run 2 RMSE = 22 pp) from deeper peats (> 45 cm depth), and overestimated decomposition (run 1 RMSE = 30 pp, run 2 RMSE = 24 pp) in shallower peat (Fig. 7).

4.2.2 Spatial variability in water table depth and peat decomposition

In all runs, peat columns with greater peat mass remaining (i.e., less decomposed peat) have WTDs that are frequently shallow or above the peat surface (Fig. 4, 5). In the Misask runs, peat mass remaining generally decreases with peat depth (Fig. 4 a, c), while the Cheinu runs have many layers of less decomposed peat overlain by highly decomposed peat (e.g., Fig. 5 c, downslope). Overall, the run 1s at both sites have less preserved, more uniform peat, with deeper, less variable water tables than the run 2s (Table 3, Fig. 4, 5, S6, S7). All runs at both sites have the highest peat mass on the midslope, less mass on the downslope and the lowest mass on the upslope (Table 3, Fig. 4 a, c and Fig. 5 a, c). Additionally, WTD are shallowest on the midslopes, and deeper on the downslopes and upslopes (Table 3, Fig. 4 b, d, Fig. 5 b, d, and Fig. S6, S7).

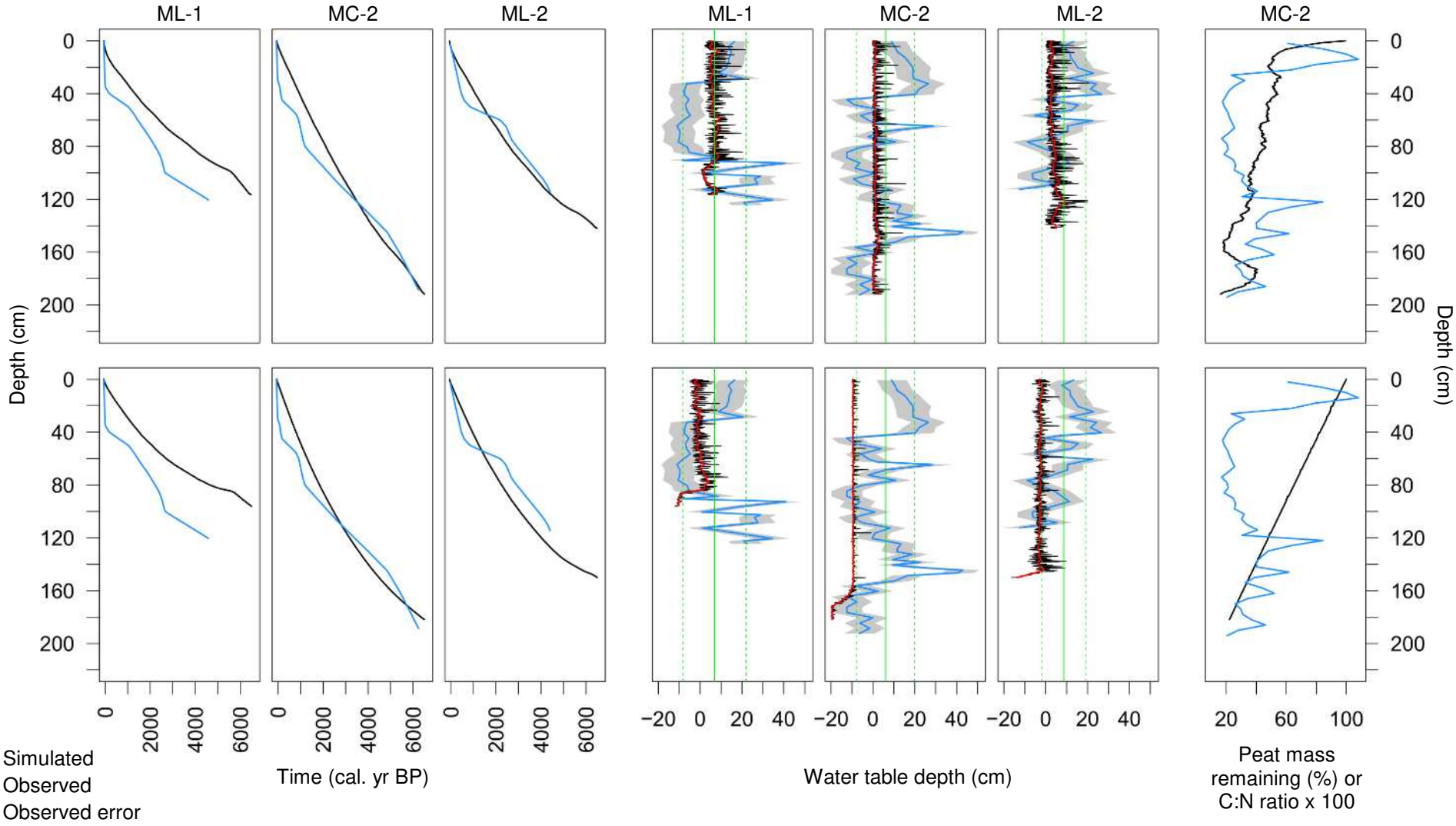

Figure 6. Misask runs 1 (top) and 2 (bottom) age-depth profiles, WTD and peat mass remaining derived from cores and simulated output at core locations. The core name is indicated on the plot. Observed peat mass remaining is based on C:N. Red lines are smoothed simulated WTDs produced with a locally-weighted polynomial regression, and green lines are the mean (solid) and mean ± 1 standard deviation (dashed) of observed WTD.

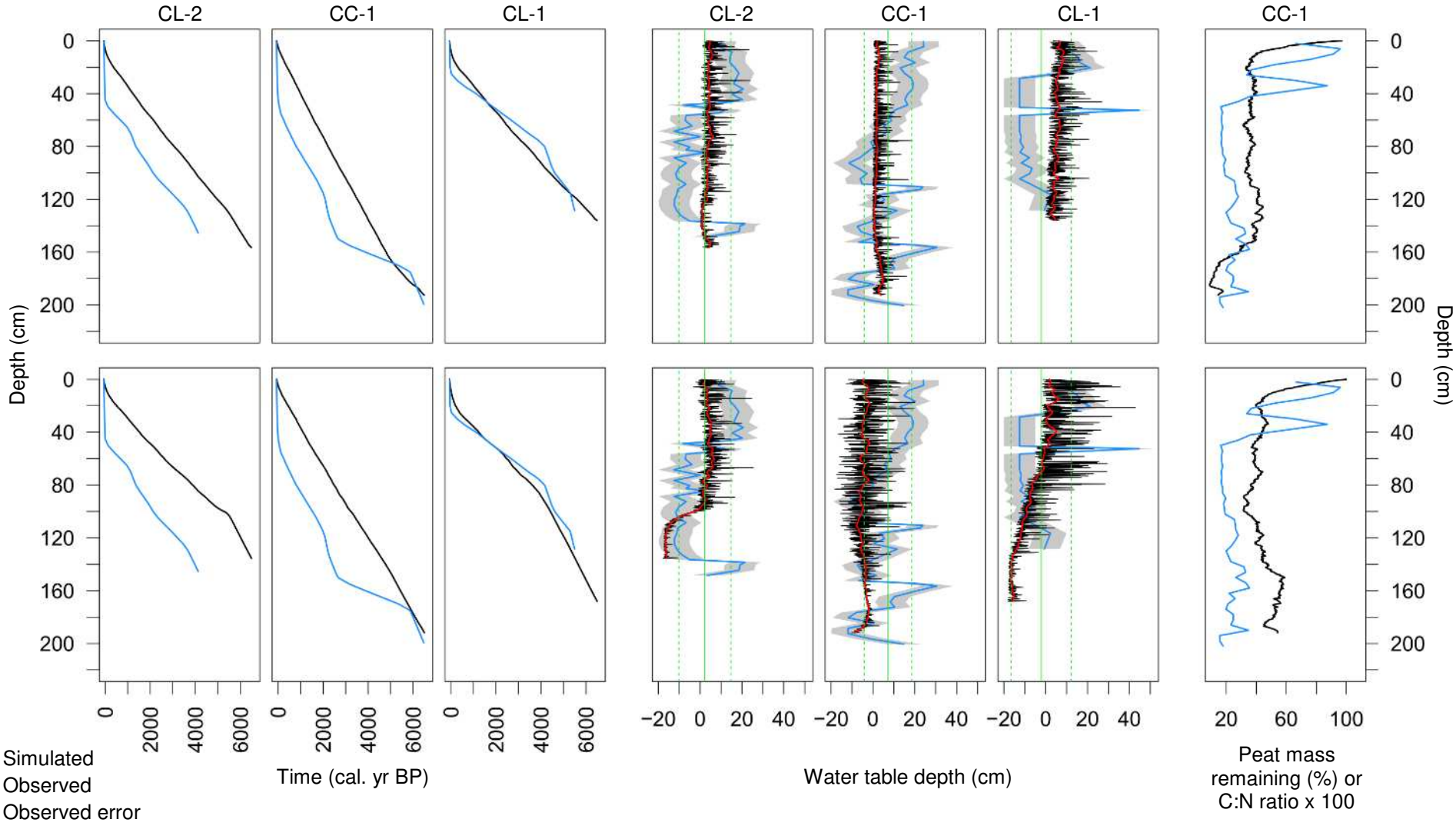

Figure 7. Cheinu runs 1 (top) and 2 (bottom) age-depth profiles, WTD and peat mass remaining derived from cores and simulated output at core locations. The core name is indicated on the plot. Observed peat mass remaining is based on C:N. Red lines are smoothed simulated WTDs produced with a locally-weighted polynomial regression, and green lines are the mean (solid) and mean ± 1 standard deviation (dashed) of observed WT

436 4.2.3 Sensitivity to the groundwater flux boundary condition

437 At both sites, run 1 peat heights responded to changes in groundwater flux when
438 compared to simulations with no groundwater flux (Fig. 8, 9 top row). Upslope peat
439 height gains occurred where additions of groundwater resulted in shallower average
440 WTDs during the growing season. Conversely, downslope peat height was thinner
441 where groundwater flux reductions produced deeper average WTDs during the
442 growing season. In these run 1s, the magnitude of peat height change was
443 commensurate with the amount of groundwater flux added or subtracted from the
444 profile (Fig. 8, 9 top row). The greatest change in peat heights occurred under
445 groundwater flux scenarios of ± 100 mm yr^{-1}. For example, under this scenario, the
446 Misask run 1 transect had a cumulative gain in peat height of 249 cm on the upslope
447 and a cumulative loss in peat height of 211 cm in the downslope. Similarly, the Cheinu
448 run 1 transect had a cumulative peat height gain of 181 cm in the upslope and a
449 cumulative peat height loss of 90 cm loss on the downslope. The response of Misask
450 run 2 to groundwater flux was minimal (Fig. 8 bottom row), with only the extreme ends
451 of the profile exhibiting changes in peat height and average growing season WTDs.
452 Peat heights on the upslope section of Cheinu run 2 responded positively to the
453 addition of groundwater, except for a column of peat 54 m from the upslope end of the
454 profile (Fig. 9 bottom row). At this location, when compared to the simulation with no
455 groundwater flux, the addition of groundwater raises the water table nearer or above
456 the peat surface, which reduces litter production, and produces thinner peat (Fig. 9
457 bottom row). Moreover, in Cheinu run 2, groundwater losses on the downslope had a
458 diminished effect on peat heights.
459

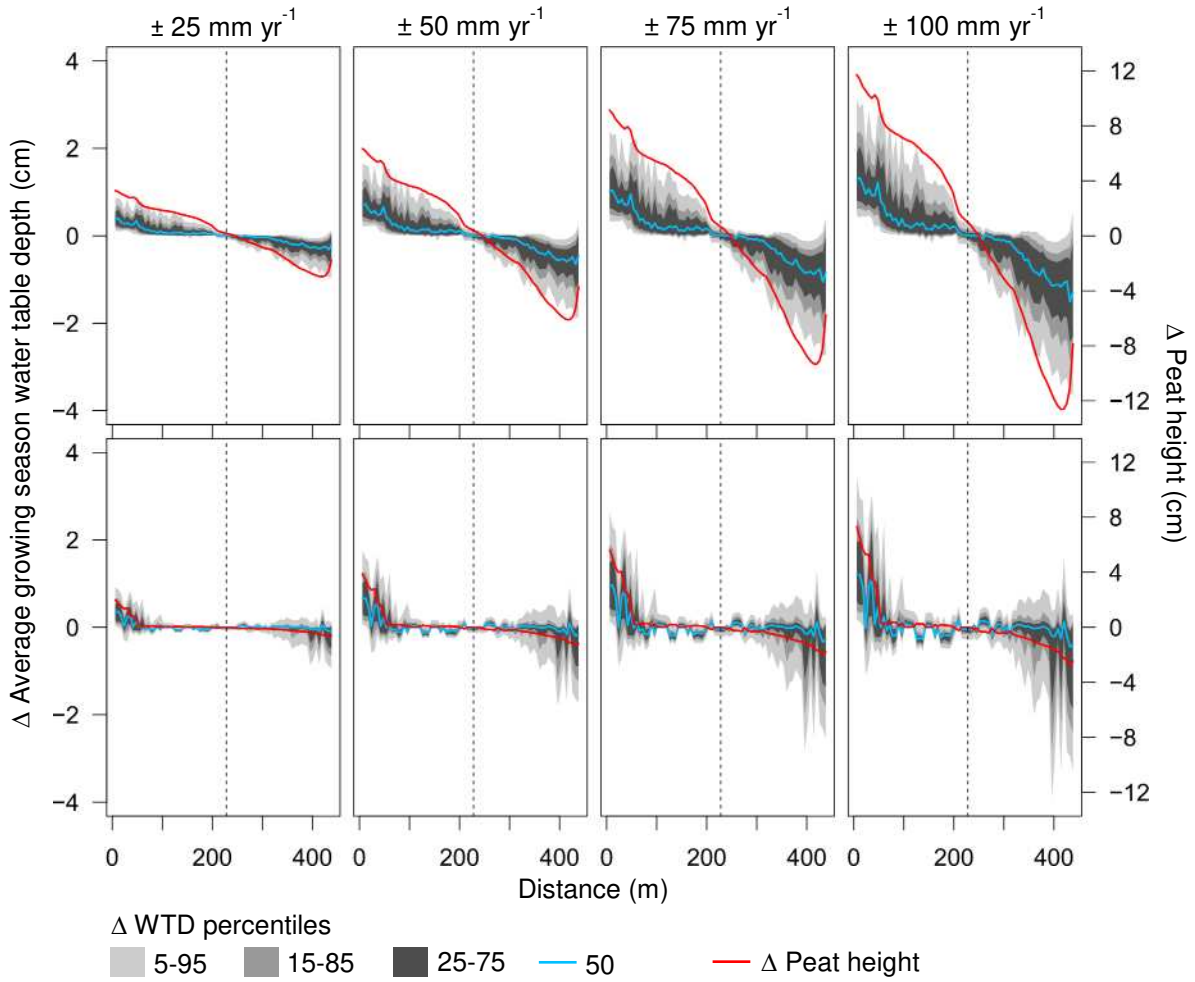

Figure 8. Misask run 1 (top row) and run 2 (bottom row) changes in all simulated annual average growing season water-table depths and changes in simulated present-day peat heights calculated between a simulation with no groundwater flux and each groundwater flux scenario. Positive changes are shallower water-table depths and gains in peat height. Groundwater gains on left side of dotted line and groundwater loses on right side of dotted line.

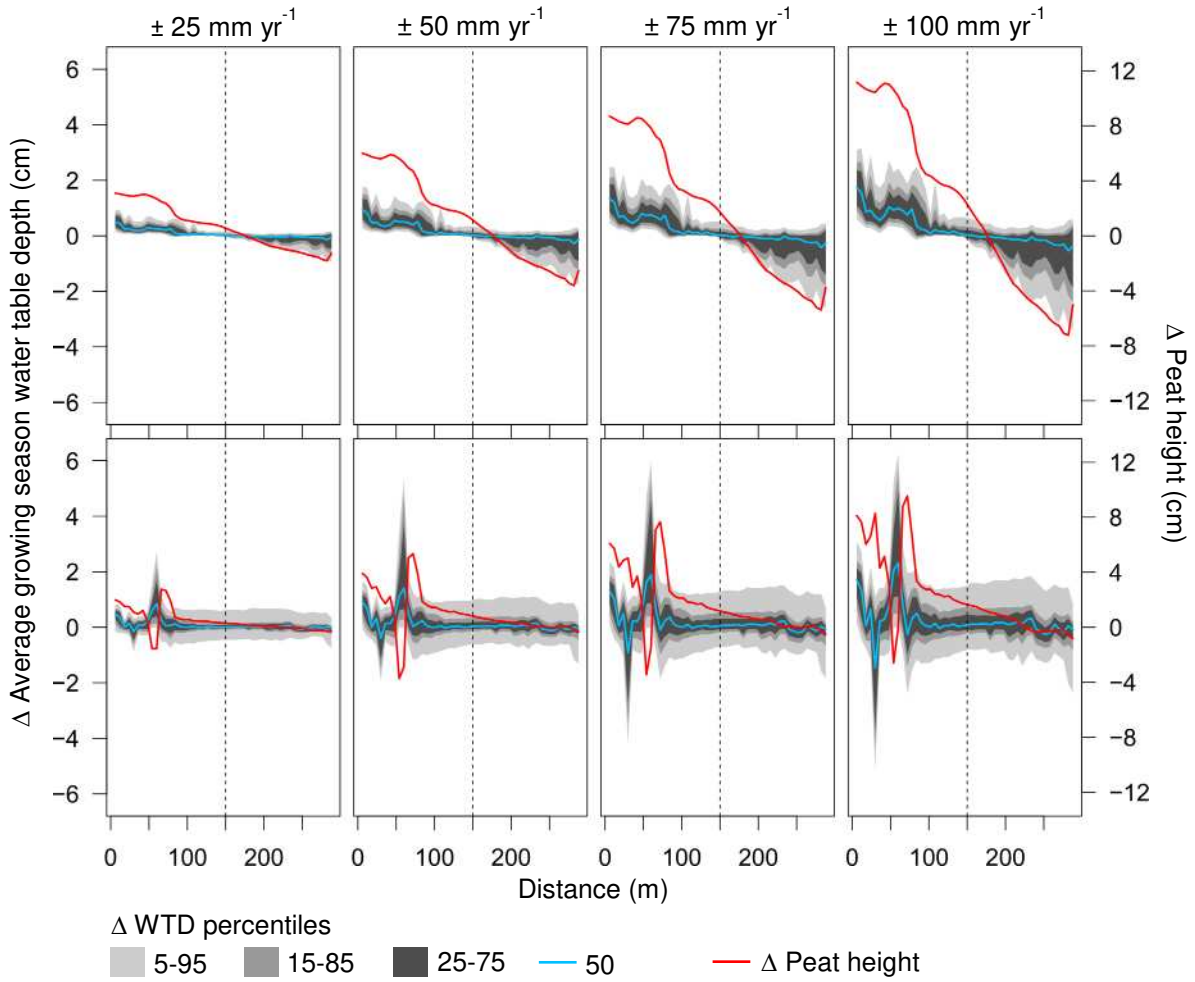

Figure 9. Cheinu run 1 (top row) and run 2 (bottom row) changes in all simulated annual average growing season water-table depths and changes in simulated present-day peat heights calculated between a simulation with no groundwater flux and each groundwater flux scenario. Positive changes are shallower water-table depths and gains in peat height. Groundwater gains on left side of dotted line and groundwater loses on right side of dotted line.

5. Discussion

Overall, the performance of the new model is mixed. In some of the simulations the peat thickness is simulated quite well (both Cheinu simulations), as are individual age-depth curves (e.g., Misask MC-2 and ML-2, both runs) and mass-remaining curves (good pattern matches for Cheinu, both runs). In contrast, water-table depths are not well simulated (all runs). The performance of the model could have been improved if we had expanded the calibration to include (i) more parameters, and (ii) the model's climatic driving data and the groundwater-exchange boundary condition. However, extending the calibration carries the risk of it becoming a curve-fitting exercise, which is of limited value in assessing the model's fidelity. Nevertheless, it is possible to identify ways in which the model and/or its climatic driving data could be enhanced. In

the case of the latter, it is likely that the variations in measured water-table depths are caused by climatic 'excursions' that are not included in our climatic driving data, which change little through time (Fig. 3). Previous work with DigiBog has shown that modelled water tables are sensitive to variations in climate (e.g., Morris et al., 2015) and we would expect the same in DigiBog_Boreal. Paleoclimatic episodes can be difficult to represent in driving data that are based solely on contemporary meteorological data and climate model hindcasts, as is the case here. Therefore, it seems likely that a lack of detail in the driving data, rather than deficiencies in the model itself, explains the poor fit between modelled and observed water tables. Below, we discuss ways in which the model itself might be improved.

In the model, simulated degree of decomposition and peat thickness are sensitive to surface-water storage (Figs. 4 and 5). Oxic-zone thickness affects both the addition of plant litter to a peat column and the decay of peat within it and is partly controlled by the size of the surface-water store as set by the model user. For example, if the surface ponding level is set to a high value, more water is stored on the peatland during and after snowmelt and this storage offsets water losses during periods of low net rainfall, ensuring water tables remain near the surface. However, litter production and peat decay in the model interact in a complicated way with water-table depth. For example, similar peat thicknesses may be attained for (i) moderate water-table depths where rates of both litter production and decay are relatively high, and (ii) shallow water-table depths where production and decay are both quite low. Similar peat thicknesses can be seen between the different surface-ponding runs for both sites, but the peat profile is very different in terms of degree of decay (the mass remaining). For example, for Misask, similar peat thicknesses are predicted for the transect between 130 m and 200 m, but the peat in the shallow-ponding run is much more decayed (less mass remaining) (Fig. 4). Nevertheless, changes in surface storage do translate into differences in peat thickness and C storage as can be seen for the beginning (0-50 m) and end (beyond 400 m) of the Misask transect (Fig. 4). Therefore, the depth to which surface water is allowed to pond can alter the simulated carbon balance. A better understanding of surface water storage and flow in these peatlands could help improve our results. Model performance may be enhanced by allowing different depths of water to be stored across different parts of the peatland, representing local surface gradients and topographic features such as hollows and ridges. Additionally, there may be merit

in explicitly modelling surface water flow within the peatland using an overland flow equation.

DigiBog_Boreal does not explicitly represent different plant functional types (PFTs); i.e., in the model, litter production and decay work at the level of the plant assemblage which is assumed to be that typical of a bog. In future versions of the model, it may be desirable to represent several PFTs that differ from each other in rates of litter production and in litter susceptibility to decay. Such changes may lead to better predictions of the downcore mass-remaining and age-depth curves. An important control on PFT is the water source; 'fen' PFTs such as some sedge species may be found in shallow peats and where some of the water supplied to the peatland is minerotrophic, such as groundwater. However, simulating shifts in PFT abundance can be challenging at sites such as Misask and Cheinu because of large uncertainties in groundwater exchanges with the peatlands over the centuries and millennia during which the peatlands develop (see Figure 8 and associated discussion). Therefore, we chose to use a simple approach to represent peatland vegetation in the first version of DigiBog_Boreal and focused instead on other controls on peatland development (growing season and snow melt).

Notwithstanding these possible upgrades and the limitations of the driving data in this test application, the new version of DigiBog already extends the model's capabilities. These capabilities suggest the approach we used here to model past peat accumulation could be used in concert with contemporary field measurements (such as C fluxes and water-table depths) and climate projections to explore the effects of land-use and climate change on boreal peatland C stocks.

6. Conclusions

We present a new version of the DigiBog model of peatland development, DigiBog_Boreal. The new model includes routines to simulate processes specific to boreal ecosystems, particularly changes to reflect the accumulation and melt of a seasonal snowpack; and changes to the routines that govern peat accumulation, to account for shorter growing seasons than in temperate ecosystems. Like previous versions of DigiBog, the new model provides a detailed, spatially-distributed representation of peat accumulation along a transect. We parameterised the model for

two peatlands in high-boreal latitudes of eastern Canada, simulating peat development over the last ~6,500 years. The model setups are informed by detailed field surveys that describe the topography of the mineral substrate upon which peat has accumulated, and radiocarbon dates from the base of the peat to the surface. Climatic driving data are provided by a general circulation model, combined with modern climate data using a weather generator. The model can be parameterised so that simulated peat thickness agrees well with observed peat profiles in both sites. Simulated peat accumulation is sensitive to the parameters used to represent the storage of water on the surface of the peat, which should therefore be well informed by field measurements. Simulated water-table depths and age-depth profiles can be compared to palaeohydrological conditions and radiocarbon age-depth profiles, respectively, reconstructed from proxy data at the two sites. In these respects, the model performs less well than for peat thickness, although we suspect this represents a lack of detail in the climatic driving data rather than deficiencies in the model's routines. Overall, the model provides a suitable means to simulate the development of boreal peatlands and may find utility in simulating the response of such ecosystems to future climate and land-use change.

7. Acknowledgements

This research was funded by NSERC in collaboration with Stornoway Diamond corporation and Nemaska Lithium to Michelle Garneau (Grant number: RDCPJ 51342-17). We are grateful to Ruza Ivanovic, Lauren Gregoire (University of Leeds) and Paul Valdes (University of Bristol) for assistance with the HadCM3 data used to drive the DigiBog simulations.

8. Data availability

DigiBog_Boreal code is available at: https://github.com/beto33014/DigiBogCanada-masterSubArcticV3 and data used in this study is available upon request.

9. References

Agnihotri, J., Coulibaly, P., 2020. Evaluation of snowmelt estimation techniques for enhanced spring peak flow prediction. Water 12, 1290.

Baird, A.J., Morris, P.J., Belyea, L.R., 2012. The DigiBog peatland development model 1: Rationale, conceptual model, and hydrological basis. Ecohydrology 5, 242–255.

Beck, H.E., Zimmermann, N.E., McVicar, T.R., Vergopolan, N., Berg, A., Wood, E.F., 2018. Present and future Köppen-Geiger climate classification maps at 1-km resolution. Sci. Data 5, 1–12.

Belyea, L.R., Clymo, R.S., 2001. Feedback control of the rate of peat formation. Proc. R. Soc. Lond. B Biol. Sci. 268, 1315–1321.
Breeuwer, A., Heijmans, M.M., Robroek, B.J., Berendse, F., 2008. The effect of temperature on growth and competition between Sphagnum species. Oecologia 156, 155–167.
Chaudhary, N., Miller, P.A., Smith, B., 2017. Modelling Holocene peatland dynamics with an individual-based dynamic vegetation model. Biogeosciences 14, 2571–2596. https://doi.org/10.5194/bg-14-2571-2017
Christidis, N., Stott, P.A., Brown, S., Karoly, D.J., Caesar, J., 2007. Human contribution to the lengthening of the growing season during 1950–99. J. Clim. 20, 5441–5454.
Fatichi, S., Ivanov, V.Y., Caporali, E., 2013. Assessment of a stochastic downscaling methodology in generating an ensemble of hourly future climate time series. Clim. Dyn. 40, 1841–1861. https://doi.org/10.1007/s00382-012-1627-2
Fatichi, S., Ivanov, V.Y., Caporali, E., 2011. Simulation of future climate scenarios with a weather generator. Adv. Water Resour. 34, 448–467. https://doi.org/10.1016/j.advwatres.2010.12.013
Fatichi, S., Peleg, N., Mastrotheodoros, T., Pappas, C., Manoli, G., 2021. An ecohydrological journey of 4500 years reveals a stable but threatened precipitation-groundwater recharge relation around Jerusalem. Sci. Adv.
Frolking, S., Roulet, N.T., Tuittila, E., Bubier, J.L., Quillet, A., Talbot, J., Richard, P.J.H., 2010. A new model of Holocene peatland net primary production, decomposition, water balance, and peat accumulation. Earth Syst. Dyn. 1, 1–21.
Garneau, M., van Bellen, S., Magnan, G., Beaulieu-Audy, V., Lamarre, A., Asnong, H., 2014. Holocene carbon dynamics of boreal and subarctic peatlands from Québec, Canada. The Holocene 24, 1043–1053.
Gordon, C., Cooper, C., Senior, C.A., Banks, H., Gregory, J.M., Johns, T.C., Mitchell, J.F., Wood, R.A., 2000. The simulation of SST, sea ice extents and ocean heat transports in a version of the Hadley Centre coupled model without flux adjustments. Clim. Dyn. 16, 147–168.
Hamon, W.R., 1961. Estimating potential evapotranspiration. J. Hydraul. Div. 87, 107–120.
Hersbach, H., Bell, B., Berrisford, P., Hirahara, S., Horányi, A., Muñoz-Sabater, J., Nicolas, J., Peubey, C., Radu, R., Schepers, D., 2020. The ERA5 global reanalysis. Q. J. R. Meteorol. Soc. 146, 1999–2049.
Hugelius, G., Loisel, J., Chadburn, S., Jackson, R.B., Jones, M., MacDonald, G., Marushchak, M., Olefeldt, D., Packalen, M., Siewert, M.B., others, 2020. Large stocks of peatland carbon and nitrogen are vulnerable to permafrost thaw. Proc. Natl. Acad. Sci. 117, 20438–20446.
Joosten, H., Clarke, D., 2002. Wise use of mires and peatlands. Int. Mire Conserv. Group Int. Peat Soc. 304.
Kim, J., Verma, S.B., 1996. Surface exchange of water vapour between an open Sphagnum fen and the atmosphere. Bound.-Layer Meteorol. 79, 243–264.
Kingsbury, C.M., Moore, T.R., 1987. The freeze-thaw cycle of a subarctic fen, northern Quebec, Canada. Arct. Alp. Res. 19, 289–295.
Lambert, C., Larocque, M., Gagné, S., Garneau, M., 2022. Aquifer-Peatland Hydrological Connectivity and Controlling Factors in Boreal Peatlands. Front. Earth Sci. 10, 835817. https://doi.org/10.3389/feart.2022.835817
Lottes, A.L., Ziegler, A.M., 1994. World peat occurrence and the seasonality of climate and vegetation. Palaeogeogr. Palaeoclimatol. Palaeoecol. 106, 23–37.
Mahdiyasa, A.W., Large, D.J., Muljadi, B.P., Icardi, M., Triantafyllou, S., 2021. MPeat—A fully coupled mechanical-ecohydrological model of peatland development. Ecohydrology e2361.
McKenney, D.W., Hutchinson, M.F., Papadopol, P., Lawrence, K., Pedlar, J., Campbell, K., Milewska, E., Hopkinson, R.F., Price, D., Owen, T., 2011. Customized spatial climate models for North America. Bull. Am. Meteorol. Soc. 92, 1611–1622.
Moore, T.R., 1989. Growth and net production of Sphagnum at five fen sites, subarctic eastern Canada. Can. J. Bot. 67, 1203–1207.
Moraga, J.S., Peleg, N., Fatichi, S., Molnar, P., Burlando, P., 2021. Revealing the impacts of climate change on mountainous catchments through high-resolution modelling. J. Hydrol. 603, 126806. https://doi.org/10.1016/j.jhydrol.2021.126806
Morris, P.J., Baird, A.J., Belyea, L.R., 2012. The DigiBog peatland development model 2: Ecohydrological simulations in 2D. Ecohydrology 5, 256–268.
Morris, P.J., Baird, A.J., Young, D.M., Swindles, G.T., 2015. Untangling climate signals from autogenic changes in long-term peatland development. Geophys. Res. Lett. 42, 10,788-10,797.
Müller, J., Joos, F., 2020. Global peatland area and carbon dynamics from the Last Glacial Maximum to the present–a process-based model investigation. Biogeosciences 17, 5285–5308.

Oudin, L., Hervieu, F., Michel, C., Perrin, C., Andréassian, V., Anctil, F., Loumagne, C., 2005. Which potential evapotranspiration input for a lumped rainfall–runoff model?: Part 2—Towards a simple and efficient potential evapotranspiration model for rainfall–runoff modelling. J. Hydrol. 303, 290–306.
Pedlar, J.H., McKenney, D.W., Lawrence, K., Papadopol, P., Hutchinson, M.F., Price, D., 2015. A comparison of two approaches for generating spatial models of growing-season variables for Canada. J. Appl. Meteorol. Climatol. 54, 506–518.
Peleg, N., Molnar, P., Burlando, P., Fatichi, S., 2019. Exploring stochastic climate uncertainty in space and time using a gridded hourly weather generator. J. Hydrol. 571, 627–641.
Qiu, C., Zhu, D., Ciais, P., Guenet, B., Peng, S., Krinner, G., Tootchi, A., Ducharne, A., Hastie, A., 2019. Modelling northern peatland area and carbon dynamics since the Holocene with the ORCHIDEE-PEAT land surface model (SVN r5488). Geosci. Model Dev. 12, 2961–2982.
Quinton, W.L., Roulet, N.T., 1998. Spring and summer runoff hydrology of a subarctic patterned wetland. Arct. Alp. Res. 30, 285–294.
Robitaille, M., Garneau, M., van Bellen, S., Sanderson, N.K., 2021. Long-term and recent ecohydrological dynamics of patterned peatlands in north-central Quebec (Canada). The Holocene 31, 844–857.
Samuel, J., Coulibaly, P., Metcalfe, R.A., 2011. Estimation of continuous streamflow in Ontario ungauged basins: comparison of regionalization methods. J. Hydrol. Eng. 16, 447–459.
Treat, C.C., Jones, M.C., Alder, J., Sannel, A.B.K., Camill, P., Frolking, S., 2021. Predicted vulnerability of carbon in permafrost peatlands with future climate change and permafrost thaw in Western Canada. J. Geophys. Res. Biogeosciences 126, e2020JG005872.
Valdes, P.J., Armstrong, E., Badger, M.P., Bradshaw, C.D., Bragg, F., Crucifix, M., Davies-Barnard, T., Day, J.J., Farnsworth, A., Gordon, C., 2017. The BRIDGE HadCM3 family of climate models: HadCM3@ Bristol v1. 0. Geosci. Model Dev. 10, 3715–3743.
Wang, X.L., Xu, H., Qian, B., Feng, Y., Mekis, E., 2017. Adjusted daily rainfall and snowfall data for Canada. Atmosphere-Ocean 55, 155–168.
Wieder, R.K., Vitt, D.H., 2006. Boreal peatland ecosystems. Springer Science & Business Media.
Wu, J., Kutzbach, L., Jager, D., Wille, C., Wilmking, M., 2010. Evapotranspiration dynamics in a boreal peatland and its impact on the water and energy balance. J. Geophys. Res. Biogeosciences 115.
Xu, J., Morris, P.J., Liu, J., Holden, J., 2018. PEATMAP: Refining estimates of global peatland distribution based on a meta-analysis. Catena 160, 134–140.
Young, D.M., Baird, A.J., Morris, P.J., Holden, J., 2017. Simulating the long-term impacts of drainage and restoration on the ecohydrology of peatlands. Water Resour. Res. 53, 6510–6522.

Supplemental material for:

Modelling peatland development in north-central Quebec, Canada with DigiBog_Boreal

Table S1. Degree-day method snowmelt model parameters.

symbol	units	range of values tried	calibrated value	description
tr	°C	0-2.5	1.8	upper threshold temperature to distinguish between rainfall and snowfall
scf	—	0.4-1.6	1.1	snowfall correction factor
ddf	mm/day °C	0-5.0	1.5	degree day factor
rcr	—	0.5-1.5	0.9	rainfall correction factor

Table S2. DigiBog_Boreal parameters that were not calibrated.

parameter	symbol	units	value	description
base temperature	T_{BC}	Celsius	6.29	arbitrary baseline temperature to define the temperature dependency of decomposition
temperature sensitivity	Q_{10}	factor (dimensionless)	2.5	The value of Q_{10} gives the factorial increase in process rate for a 10°C increase in temperature (e.g., Q_{10} = 2 means a doubling of the process rate of interest for every 10°C increase).
dry bulk density	ρ	g cm^{-3}	0.1	peat bulk density
drainable porosity	*s*	proportion	0.3	drainable porosity
hydraulic conductivity parameter	*a*	cm yr^{-1}	31737.45	*a* and *b* are parameter values that describe the shape of the relationship between time-integrated decomposition and hydraulic conductivity.
hydraulic conductivity parameter	*b*	dimensionless	8	

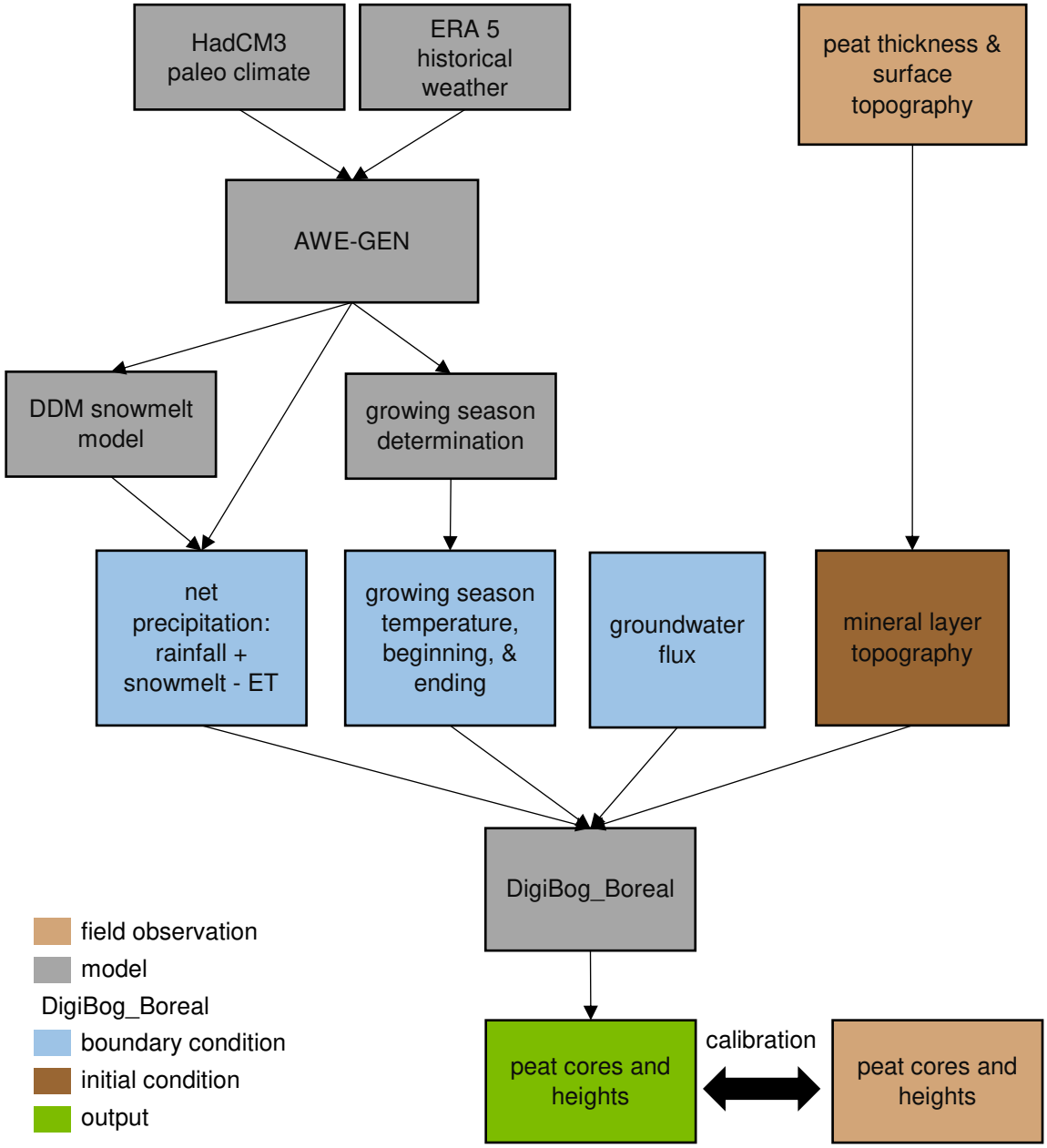

Figure S1. Flowchart of DigiBog_Boreal setup.

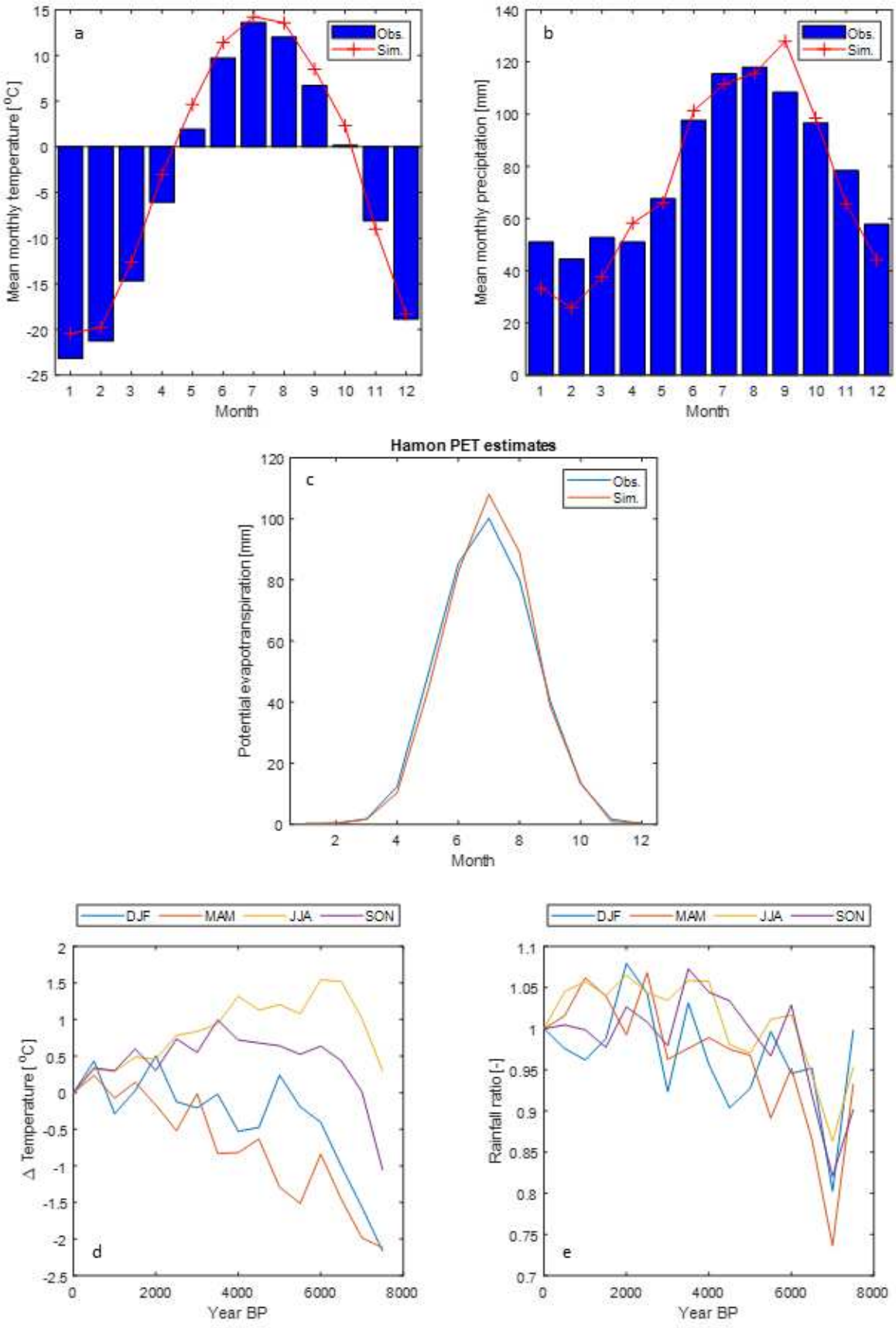

720

721 **Figure S2.** Validation of simulated average monthly temperature (a), precipitation (b)
722 and PET (c) for the CE period. Computed FC for temperature (difference, d) and
723 precipitation (ratio, e) from the HadCM3 model.

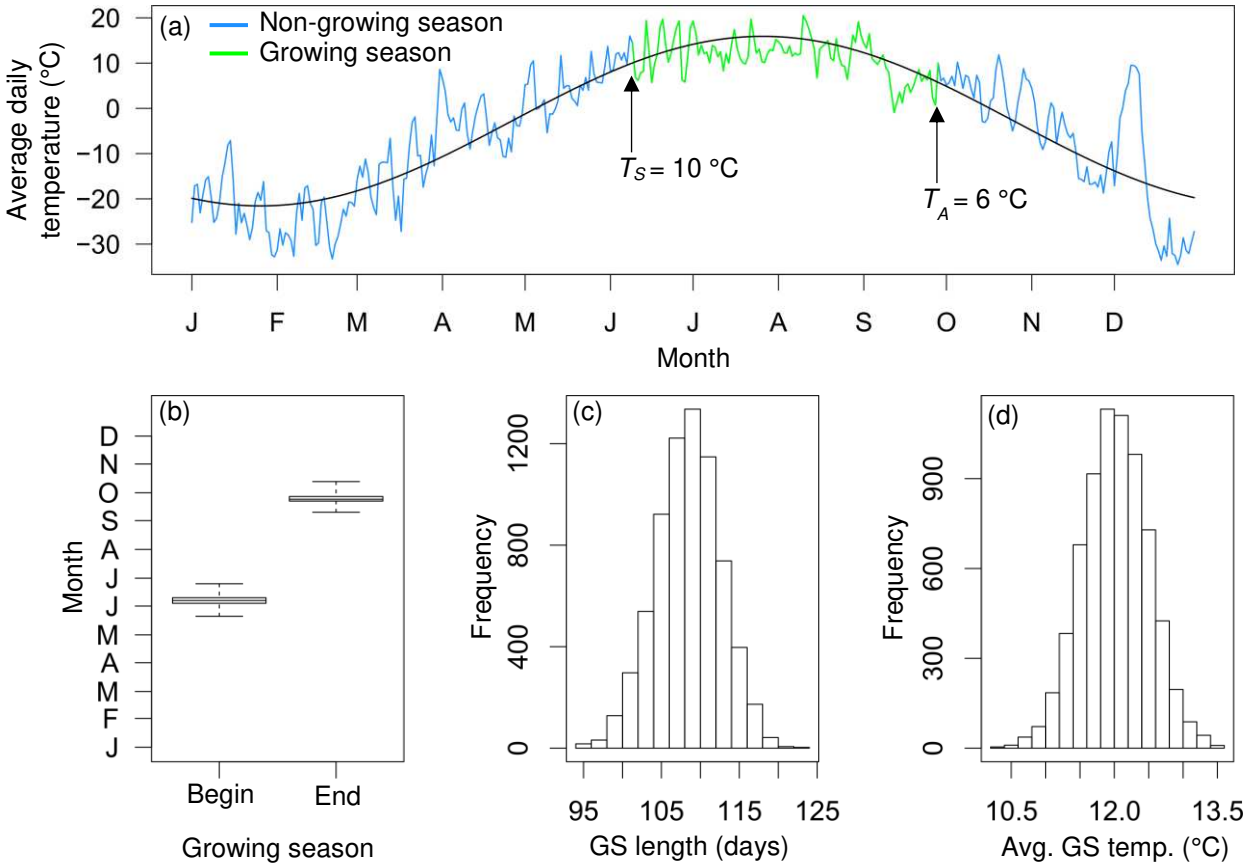

Figure S3. Example of one growing season (GS) derived from simulated present-day climate, where the growing season begins the first day in the year when smoothed daily average temperature (black line) is > T_S and ends the first day in the year smoothed daily average temperature is < T_A (a). Summary of growing seasons derived from 7000 years of simulated present-day climate (1981-2019) (b-d).

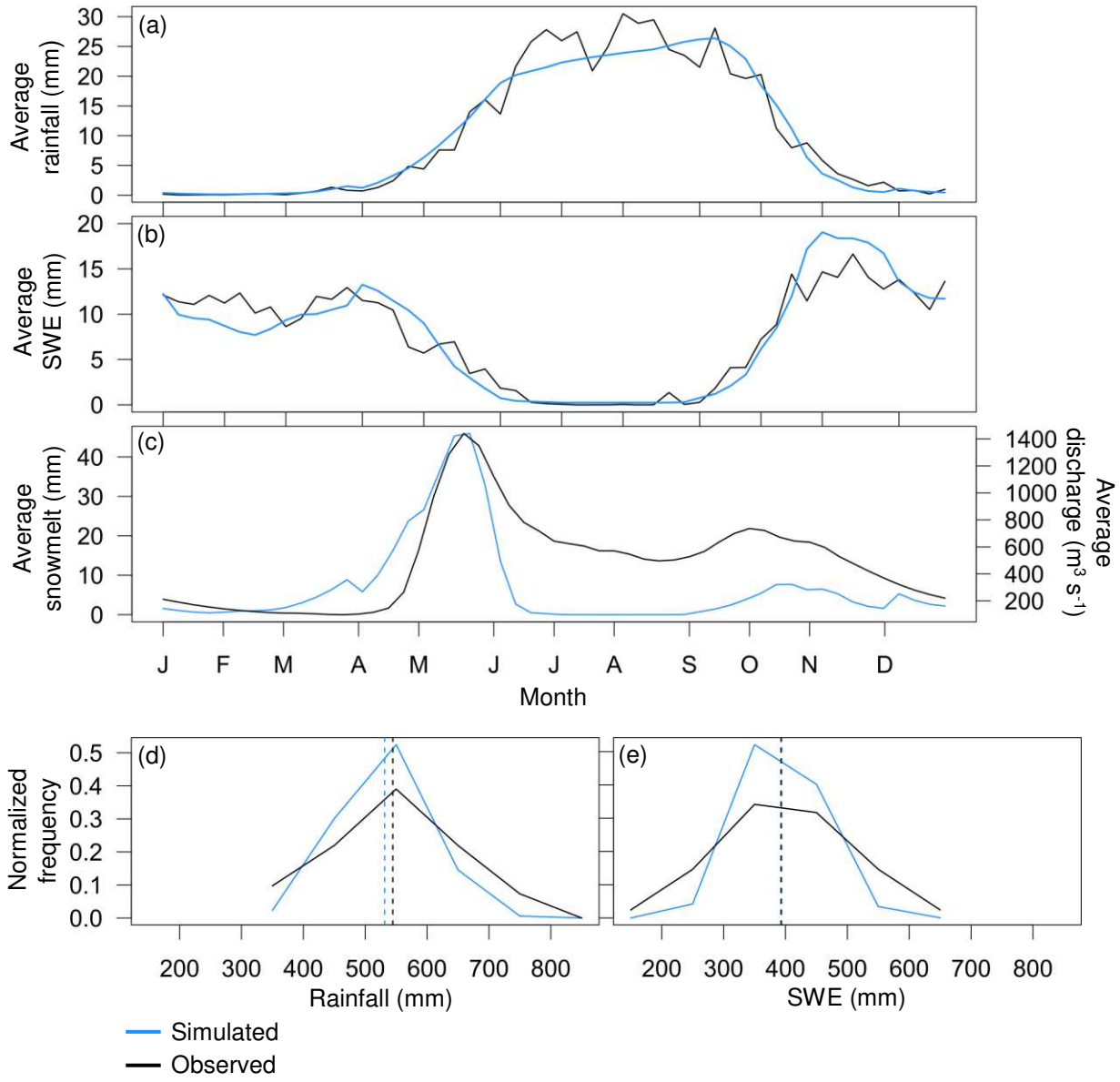

Figure S4. Observed and simulated weekly total rainfall (a) and snow water equivalent (SWE). Simulated weekly total snowmelt (blue line) and observed river discharge (black line) measured at the nearest downstream gauging station on the Eastmain river (Gorge Prosper gauging station (1981-2000)) (c). Distributions of observed and simulated total annual rainfall (d) and SWE (e). Dashed lines indicate the distribution mean.

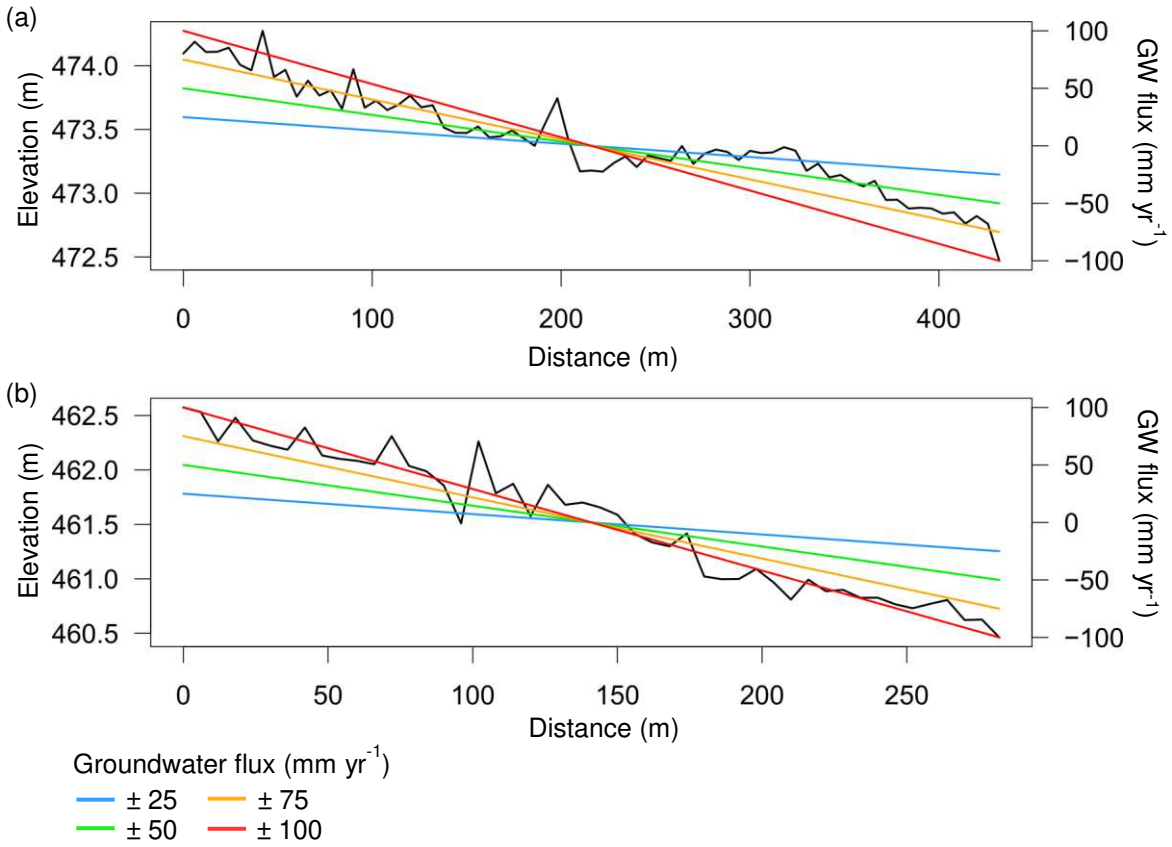

Figure S5. Simulated groundwater (GW) flux applied to the Misask (a) and Cheinu (b) transects. Observed peat surface as a black line.

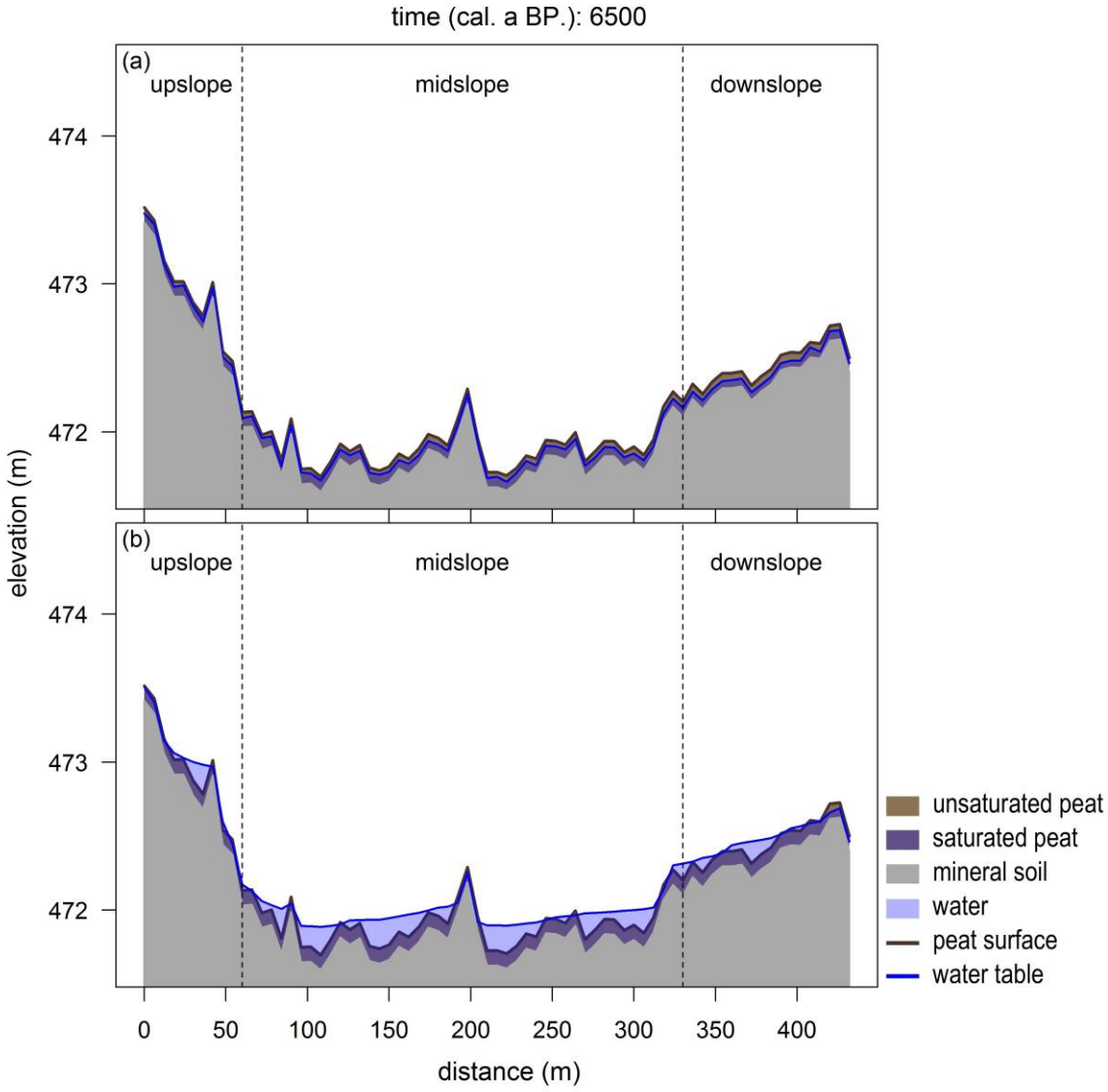

Figure S6. Animated profile view of 6566 years of annual peat height and average growing season water table height for Misask run 1 (a) and 2 (b), video accessible at: https://figshare.com/articles/media/Misask_peatland_DigiBog_Boreal_simulation/18040118. Non-growing season water table not included in the animation.

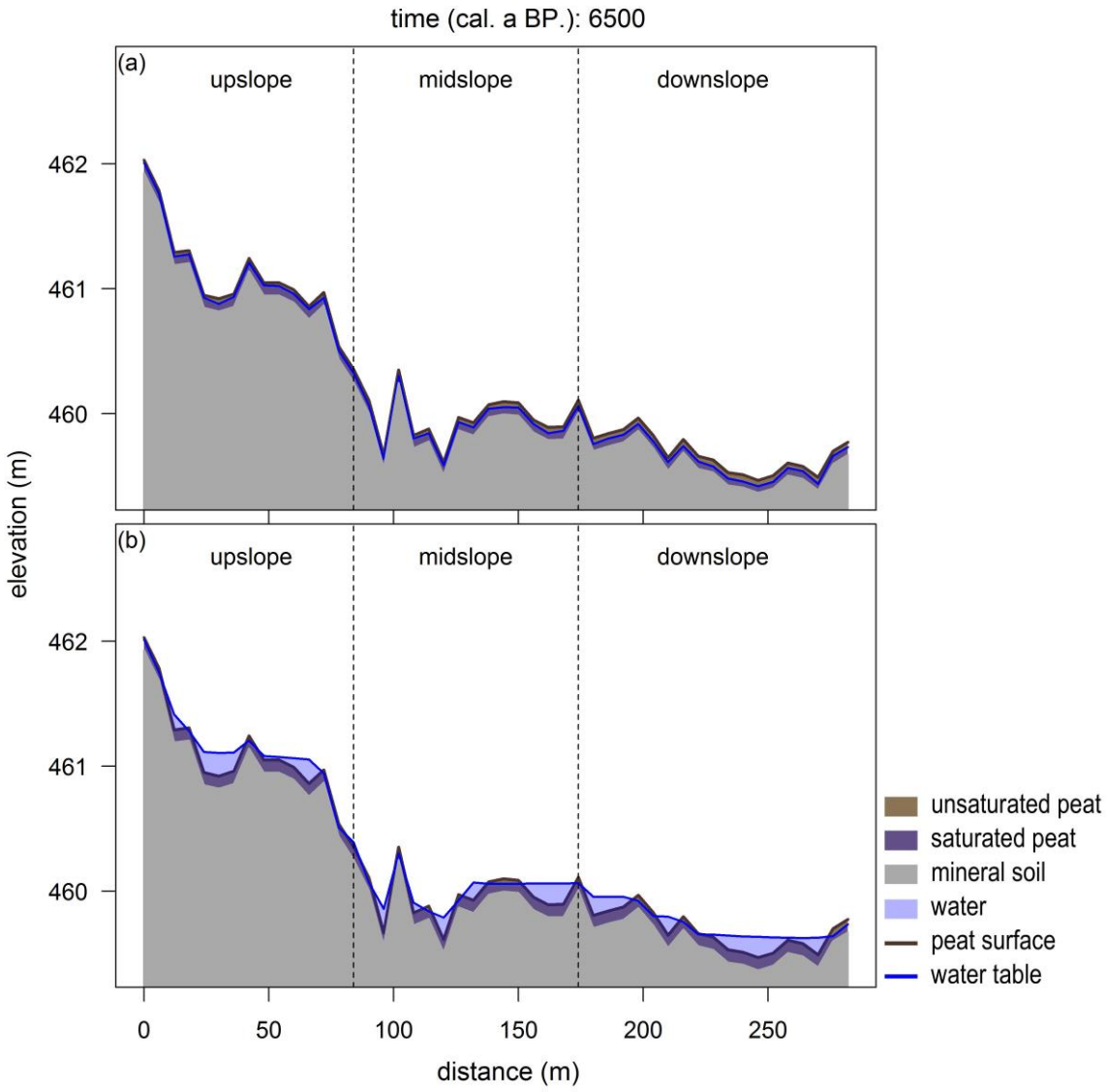

Figure S7. Animated profile view of 6566 years of annual peat height and average growing season water table height for Cheinu run 1 (a) and 2 (b), video accessible at: https://figshare.com/articles/media/Cheinu_peatland_DigiBog_Boreal_simulation/18041357. Non-growing season water table not included in the animation.

References

Morris, P.J., Baird, A.J., Young, D.M., Swindles, G.T., 2015. Untangling climate signals from autogenic changes in long-term peatland development. Geophysical Research Letters 42, 10,788-10,797.